LIMNOLOGY and OCEANOGRAPHY

ASLO

Limnol. Oceanogr. 65, 2020, 1990–2009

doi: 10.1002/lno.11432

Role of delta-front erosion in sustaining salt marshes under sea-level rise and fluvial sediment decline

Shi Lun Yang,[1,2]* Xiangxin Luo,[3] Stijn Temmerman,[4,†] Matthew Kirwan,[5,†] Tjeerd Bouma,[6,†] Kehui Xu,[7] Saisai Zhang,[1] Jiqing Fan,[1] Benwei Shi,[1,7] Haifei Yang,[1] Ya Ping Wang,[1] Xuefa Shi,[8] Shu Gao[1,2]

[1]State Key Laboratory of Estuarine and Coastal Research, East China Normal University, Shanghai, China
[2]Institute of Eco-Chongming, East China Normal University, Shanghai, China
[3]Institute of Estuarine and Coastal Research, Sun Yat-sen University, Guangzhou, China
[4]Ecosystem Management Research Group, University of Antwerp, Antwerp, Belgium
[5]Virginia Institute of Marine Science, William & Mary Gloucester Point, Williamsburg, Virginia, USA
[6]Department of Estuarine and Delta systems, Royal Netherlands Institute for Sea Research (NIOZ), Utrecht University, Yerseke, The Netherlands
[7]Department of Oceanography and Coastal Sciences, Louisiana State University, Baton Rouge, Louisiana, USA
[8]Key Laboratory of Marine Sedimentology and Environmental Geology, First Institute of Oceanography, State Oceanic Administration, Qingdao, China

Abstract

Accelerating sea-level rise and decreasing riverine sediment supply are widely considered to lead to global losses of deltaic marshes and their valuable ecosystem services. However, little is known about the degree to which the related erosion of the seaward delta front can provide sediments to sustain salt marshes. Here, we present data from the mesomacrotidal Yangtze Delta demonstrating that marshes have continued to accrete vertically and laterally, despite rapid relative sea-level rise (~10 mm yr^{-1}) and a > 70% decrease in the Yangtze River sediment supply. Marsh progradation has decelerated at a lower rate than fluvial sediment reduction, suggesting an additional source of sediment. We find that under favorable conditions (e.g., a mesomacrotidal range, strong tidal flow, flood dominance, sedimentary settling lag/scour lag effects, and increasing high-tide level), delta-front erosion can actually supply sediment to marshes, thereby maintaining marsh accretion rates in balance with relative sea-level rise. Comparison of global deltas illustrates that the ability of sediment remobilization to sustain marshes depends on coastal processes and varies by more than an order of magnitude among the world's major deltas.

Salt marshes are among the world's most valuable ecosystems (Costanza et al. 1997). They sequester carbon, protect shorelines from storm impacts, transform nutrients, contribute to fisheries production, and maintain biodiversity (Barbier et al. 2011; Kirwan and Megonigal 2013; Temmerman et al. 2013; Möller et al. 2014). Unfortunately, many salt marshes have disappeared due to reclamation and waste disposal during the past century (Gedan et al. 2009; Ma et al. 2014). Deltaic marshes are one of the most dynamic landscapes on Earth's surface (Wagner et al. 2017) and are threatened by accelerating sea-level rise and decreases in fluvial sediment supply. Decreasing fluvial sediment supply reduces the ability of salt marshes to accumulate sediments and to build up their soil elevation in balance with the rising sea level (Kirwan et al. 2010; Weston 2014). Although the morphology and evolution of deltas are influenced by various factors (Paola et al. 2011), such as riverine water and sediment discharges (Besset et al. 2019), sediment properties (Caldwell and Edmonds 2014), flow patterns (Shaw et al. 2016), vegetation height and density (Nardin et al. 2016), marine hydrodynamics (waves, tides, and longshore currents) (Caldwell and Edmonds 2014; Besset et al. 2017), land subsidence and sea-level changes (Jerolmack 2009; Syvitski et al. 2009), changes in the fluvial sediment supply and relative sea level are usually the most important for the long-term morphological evolution of deltaic marshes. The rate of global mean sea-level rise increased from 1.4 mm yr^{-1} between 1880 and 1993 to 2.9 mm yr^{-1} between 1993 and 2010 (Church and White 2011), and projections

*Correspondence: slyang@sklec.ecnu.edu.cn

Additional Supporting Information may be found in the online version of this article.

[†]Author Contribution Statement: S.T., M.K., and T.B. contributed equally to this work.

suggest that it will most likely continue to accelerate to a value of 3–15 mm yr^{-1} by 2100 (IPCC 2013). Additionally, the sediment discharges of the world's rivers have declined substantially since the 1950s due to dam construction, water diversion, and soil conservation (Syvitski et al. 2005; Dai et al. 2009; Milliman and Farnsworth 2011; Wang et al. 2011). In many cases, the fluvial sediment supply to the coast has decreased to nearly zero (Vörösmarty et al. 2003; Walling 2006; Besset et al. 2019).

Several studies have been conducted to assess salt marsh sustainability in the face of sea-level rise and fluvial sediment decline (Blum and Roberts 2009; Kirwan et al. 2010; Reed 1995; Rizzetto and Tosi 2011; Schuerch et al. 2018). For example, numerical models predict that many coastal wetlands will be inundated by the end of the present century if suspended sediment concentrations (SSCs) are below 0.01–0.02 kg m^{-3} (Moeslund et al. 2011; Blankespoor et al. 2014; Spencer et al. 2016). In contrast, models suggest that salt marshes could escape from drowning under a wide range of future sea-level rise scenarios (ranging from 10 to 50 mm yr^{-1}) in areas where river sediment delivery to the coast is not restricted by dams (French 2006; Kirwan et al. 2010; Kirwan et al. 2016*a*). Sediment availability also influences the lateral evolution of wetlands, including the expansion of interior ponds and the rate of marsh edge progradation or erosion (Mariotti et al. 2010; Kirwan et al. 2016*b*; Schepers et al. 2017; Ganju et al. 2017). Thus, sediment availability is widely identified as a major determinant of salt marsh sustainability in the face of sea-level rise. While much attention has been paid to reductions in fluvial sediment supply (Syvitski et al. 2009; Giosan et al. 2014; Yang et al. 2018*b*; Besset et al. 2019), little is known about the contributions of seaward sediment sources (Ganju et al. 2017) or the extent to which sediment mobilized by nearshore erosion can compensate for reduced fluvial sediment discharge in sustaining coastal wetlands. Previous studies found that erosion in some parts of a delta tended to be balanced by deposition in other parts of the delta system (e.g., Anderson et al. 2014; Carlin and Dellapenna 2014; Anthony 2015; Jalowska and Mckee 2017). However, the role of delta-front erosion in supplying sediment and thereby neutralizing the impacts of sea-level rise and fluvial sediment decline on salt marshes remains unclear. Specifically, little is known about the linkage between delta-front erosion and salt marsh accretion.

We address this knowledge gap by studying the Yangtze Delta as a model system, as it represents one of the world's largest deltas in terms of size, population, and economy, and its wetland areas (Fig. 1) are threatened by both rapid relative sea-level rise and a dramatic decrease in the fluvial sediment supply in recent decades (Bianchi and Allison 2009; Syvitski et al. 2009; Tessler et al. 2015). Although previous studies have assessed the direct impacts of sea-level rise and fluvial sediment decline on coastal wetlands (Blum and Roberts 2009; Rizzetto and Tosi 2011; Tessler et al. 2015), our study is unique in that it focuses on the ability of sediment derived from delta-front erosion to sustain salt marshes.

Common methods available for studying morphological evolution in delta and coastal marsh systems include (1) dating of sediment cores to calculate deposition rates (Törnqvist et al. 2008; Wang et al. 2018); (2) comparison of shorelines, isobaths, or vegetation boundaries on topographic maps (Fanos 1995; Yang et al. 2011) or remote sensing images (Anthony 2015; Shaw et al. 2016) from different time periods to illustrate and compute lateral progradation/retreat rates; (3) comparison of coastal profiles surveyed in different years to illustrate and calculate vertical accretion/erosion and lateral progradation/retreat rates (Yang et al. 2002; van Maren 2005); (4) use of digital elevation model and geographic information system (GIS) technology to show spatial variations in accretion/erosion (Shaw et al. 2016; Luo et al. 2017); (5) creation of hydrodynamic-morphodynamic models, in particular Delft3D, to simulate and predict morphological evolution in deltas and coastal wetlands (Caldwell and Edmonds 2014 ; Nardin et al. 2016; Luan et al. 2017); and (6) identification of temporal coarsening of surface sediment to infer delta erosion (Guillen and Jimenez 1995; Luo et al. 2012; Yang et al. 2018*a*). These methods are mutually complementary. For example, the advantage of the core dating method is that it provides deposition rates in the absence of topographic/bathymetric data. It is most useful in studying Holocene delta evolution. However, it is difficult to identify delta erosion using this method. Theoretically, the application of numerical models is not subject to temporal or geographical constraints, but the reliability of the results of this method is highly dependent on the accuracy of various parameters, such as flow velocity and direction, tidal range, wave height, water depth, SSC, grain size distribution, salinity, water and sediment density, temperature, et al. Most of these parameters are highly variable in time and space, making them difficult to model accurately.

In this study, we used a comprehensive methodology for understanding the role of delta-front erosion in supplying sediment to sustain salt marsh accretion under fluvial sediment decline and sea-level rise. We collected remote sensing images of coastal wetlands and data on riverine water and sediment discharges, subaqueous delta bathymetry, sea-level rise, tidal range, and wave height over the past five decades. We measured time series of current velocity and direction, wave height, and SSC during tidal cycles both in the coastal wetland and the subaqueous delta, and repeatedly surveyed elevations in the coastal wetland (monthly to 8-year intervals) using state-of-the-art instruments. We also measured SSC in the upper estuary, lower estuary, and delta front (twice a day for two decades). We calculated combined current–wave bed shear stress, flood and ebb sediment fluxes, and time-averaged rates of erosion and progradation/accretion in both the coastal wetland and the subaqueous delta. We thereby evaluated the contribution of sediments derived from delta-front erosion to salt marsh accretion. We also discussed the differences in coastal processes and the potential of erosion-derived sediment to sustain salt marshes among the world's deltas.

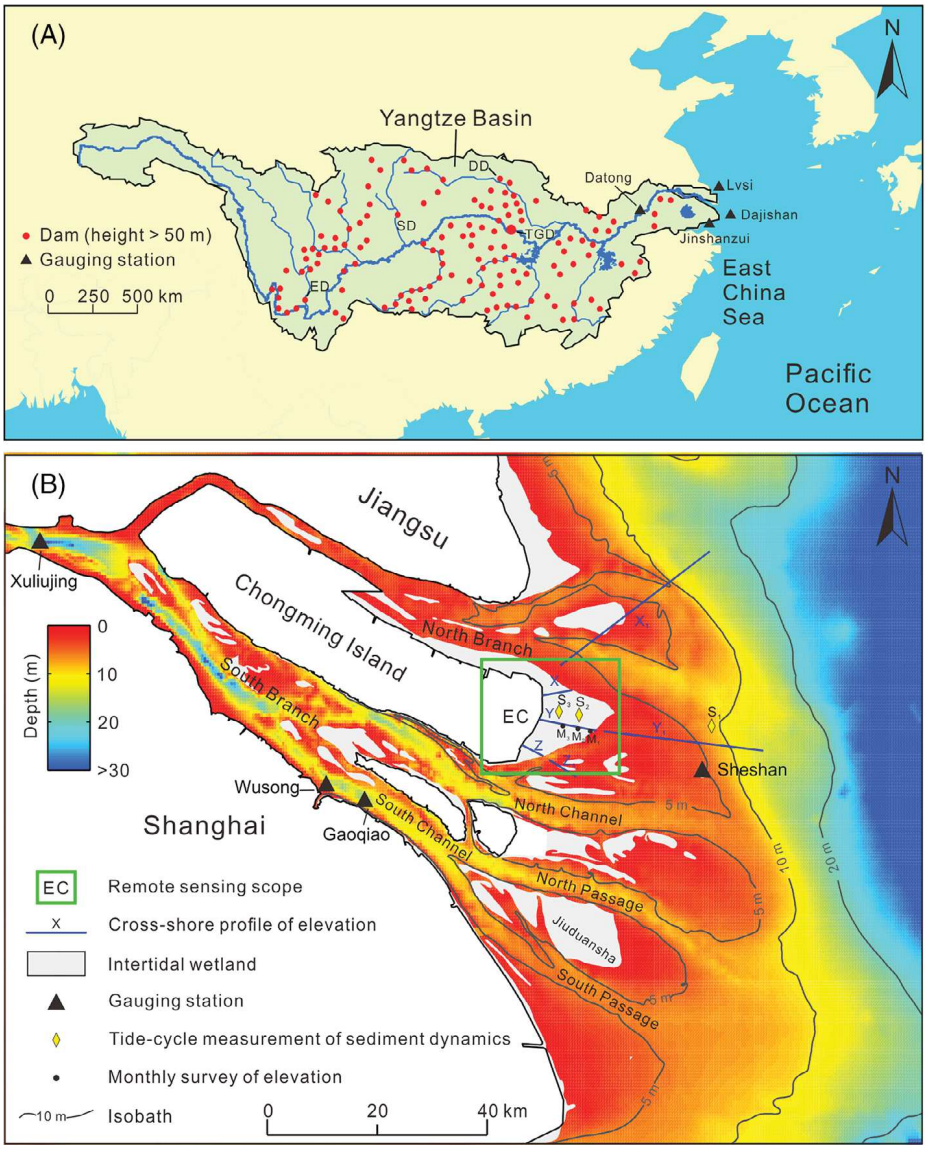

Fig. 1. Maps of the Yangtze River Basin and the Yangtze Delta. (**A**) The Yangtze Basin showing the distribution of major dams (> 50 m high) constructed since the 1950s, the location of the most seaward gauging station for water and sediment discharge (Datong, the tidal limit), and the locations of three gauging stations for sea level in the delta front (Lvsi, Dajishan, and Jinshanzui). Among the numerous dams, the Danjiangkou Dam (DD), Shengzhong Dam (SD), Ertan Dam (ED) and TGD have played the most important roles in the decline of the Yangtze sediment discharge over different historical periods (see Fig. 2B). Detailed information on the four dams is provided in Table S2. **(B)** the modern Yangtze Delta showing the locations of the studied intertidal wetlands in Eastern Chongming (EC) and adjacent subaqueous areas. Depth is relative to the lowest astronomic tide. X, Y, Z, X_1, Y_1, and Z_1 represent cross-shore elevation profiles surveyed in decadal intervals. S_1, S_2, and S_3 represent sites of hydrodynamic and sedimentary measurements in the subaqueous delta, mudflat and salt marsh, respectively. M_1, M_2, and M_3 represent sites of monthly elevation surveys in the intertidal wetland. Wusong and Gaoqiao are gauging stations for sea-level within the Yangtze Estuary. Xuliujing, Gaoqiao, and Sheshan are gauging stations where the SSC have been measured twice per day since 1998. Sheshan is also a gauging station for tidal level and tidal range. The intertidal wetlands in Eastern Chongming and Jiuduansha are the world and national nature reserves.

Materials and methods

Regional background

The Yangtze River has the world's largest watershed population (450 million) and ranks ninth in drainage area (1.8 million km^2), third in length (6300 km), fifth in water discharge (900 km^3 yr^{-1}), and fourth in sediment discharge (500 Mt yr^{-1} before the decline since the 1970s) (Milliman and Farnsworth 2011; Yang et al. 2015). The subaerial delta, which has been built up by sediment deposition from the Yangtze since the mid-Holocene, is nearly 100,000 km^2, supports 8% of China's population and provides 15% of China's gross domestic product (Wang et al. 2018; Xu et al. 2014). Sediments in the Yangtze subaqueous delta are composed mainly of silt and clay (Wang et al. 2018). Tides in the Yangtze Delta are semidiurnal with diurnal inequality. The tidal range is

approximately 2.7 m on average but increases to 4 m during spring tides. Intertidal wetlands are widely distributed in this delta. Some of them are greater than 10 km in width. More than 98% of the Yangtze's water and sediment discharges into the sea through the three outlets of the South Branch. Off the Yangtze River mouth, on the inner continental shelf, a strong southward longshore current develops, particularly under the influence of northerly winds in winter (Liu et al. 2014).

The tidal wetlands in Eastern Chongming Island and Jiuduansha shoal are the two largest (each with an area > 200 km^2) (Fig. 1B). Both are national nature reserves, and the wetlands in Eastern Chongming are listed in the Ramsar Convention on Wetlands. Salt marsh vegetation in the Yangtze Delta was originally dominated by two native species, *Scirpus mariqueter* (in the lower marsh) and *Phragmites australis* (in the higher marsh). However, *Spartina alterniflora* was introduced in the northern part of Eastern Chongming in 2003. *S. alterniflora* can grow from low to high marshes. By 2013, the northern marshes in Eastern Chongming were dominated by *S. alterniflora* because its competitive ability is greater than those of the two native plant species (personal observations). The heights of *S. mariqueter, P. australis* and *S. alterniflora* are approximately 0.5, 1.5, and 1.5 m, and their dry biomasses are 0.4, 2.7, and 3.7 kg m^{-2}, respectively (Li and Yang 2009).

Data mining

The data on the annual discharges of water and suspended sediment measured at Datong Station, which is located at the tidal limit, were obtained from the Changjiang (Yangtze) Water Resource Committee (http://www.cjw.gov.cn/zwzc/bmgb/nsgb). These data are based on daily measurements of section-averaged flow velocities and SSCs (Yang et al. 2014). The global mean sea-level data from 1965 to 2010 were obtained from Church and White (2011), whereas the global mean sea-level data from 2010 to 2017 were collected from the National Oceanic and Atmospheric Administration of the United States (2018). The mean sea-level data for the Yangtze Delta were based on measurements at five gauging stations (Fig. 1). The sea-level data at these stations between 1965 and 1979 were from Li et al. (1998), whereas the sea-level data between 1980 and 2017 were from the State Oceanic Administration (SOA), People's Republic of China (2018). The tidal range and high tidal-level data at Sheshan Station were obtained from the Forecast Center for East China Sea. The data on land subsidence in the Yangtze Delta, based on repeated surveys of land surface elevation relative to bedrock marks at 34 fixed sites, were collected by the Shanghai Municipal Planning and Land Resources Administration (2018). Considering that the sediment discharge from the Yangtze began to decrease at the end of the 1960s (Yang et al. 2002; Fig. 2B), we used an aerial photograph taken in 1965 and four Landsat images taken in 1988, 1995, 2003, and 2013 (Table S1) to delineate the low marsh edges in Eastern Chongming in different years and to calculate time-averaged rates of marsh progradation in different periods. The aerial photograph was taken by the Shanghai Aerial Survey Bureau. The Landsat images were collected from the Computer Network Information Center, Chinese Academy of Sciences (http://www.gscloud.cn/). We selected these images based on the following three principles: (1) the images should have been taken in summer (when the

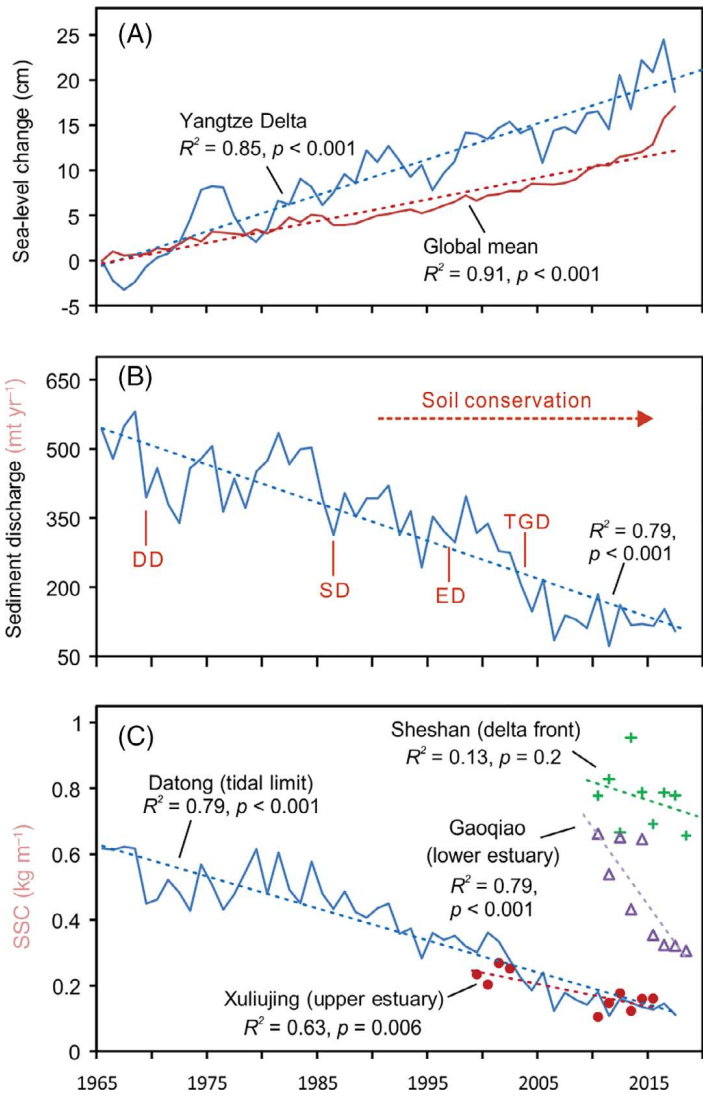

Fig. 2. The sea-level rise in the East China Sea and decrease in sediment supply from the Yangtze River. (**A**) Annually averaged sea-level changes in the Yangtz Delta compared with the global mean sea-level change (1965–2016), both showing a significantly increasing trend. The linear trend in the sea-level in the Yangtze Delta suggests an overall sea-level rise rate of 4.0 mm yr^{-1}, whereas the temporal trend in the global mean sea-level suggests a rate of 2.4 mm yr^{-1}. (**B**) Annual sediment discharge (Q_s) measured at Datong (located at the tidal limit) (1965–2016) showing a significant decreasing trend. The symbols ED, SD, DD, and TGD indicate the Ertan, Shengzhong, Danjiangkou, and Three Gorges Dams, respectively (see Fig. 1 for the locations and Table S2 for detailed information of these dams). (**C**) Annually averaged SSC measured at Datong (1965–2016), Xuliujing (upper estuary) (1998–2014 with an interruption from 2002–2008), Gaoqiao (lower estuary) (2009–2017), and Sheshan (delta front) (2009–2017), based on analysis of daily water samples. The SSC at Datong, Xuliujing, and Gaoqiao all show a significantly decreasing trend, whereas the concentration at Sheshan shows a nonsignificant decreasing trend.

marsh vegetation flourishes), at low tide (when the marsh is entirely exposed), and under cloud-free conditions; (2) the number of images should be four or more, because we needed at least three time-averaged rates of marsh progradation to find a correlation between progradation rate and fluvial sediment discharge; (3) to reduce the error in calculating time-averaged rates of marsh progradation, the time interval between two images should be longer than 5 years. In the aerial photograph and the satellite images, the boundary between the areas of marshlands and mudflats was clearly identifiable. The bathymetry in the subaqueous portions of the delta was surveyed by the Maritime Survey Bureau of Shanghai, Ministry of Communications of China, using an echo sounder with a precision of 0.1 m and a global positioning system (GPS) device with a horizontal error of ± 0.5 m. The wind speed and wave height data at the nearshore station (Sheshan) were obtained from the European Centre for Medium-Range Weather Forecasts (https://www.ecmwf.int/).

Morphological measurements and sediment sampling

The marsh–mudflat boundaries identified in the satellite images and aerial photograph were verified in the field. The elevations along three cross-shore wetland profiles in Eastern Chongming (X, Y, and Z; see Fig. 1B) were synchronously surveyed in June 2005 and June 2013, and the elevations at three fixed sites along Profile Y (M_1, M_2, and M_3) were surveyed each month from June 2005 to June 2013, using high-resolution, high-accuracy, real-time kinematic GPS units (Trimble Company) with horizontal and vertical errors of ± 10 mm + 1 ppm (parts per million) RMS (Root Mean Square) and ± 20 mm + 1 ppm RMS, respectively. All surveys were based on the same reference benchmark that was built into a concrete seawall at the starting point of the central cross-shore profile (Profile Y), and all repeated surveys of elevation were conducted at fixed sites in the wetlands. Surface sediments were sampled from the seabed using a grab sampler. Core sediments were sampled along the cross-shore wetland profiles using Polyvinyl chloride pipes 5 cm in diameter.

Hydrodynamic and SSC measurements

Under normal weather (nonstorm) conditions in September 2009, current profiles were measured using self-logging pulse-coherent acoustic Doppler current profilers (PC-ACDPs, SonTek) with the sensor probes facing downward and acoustic Doppler profilers (ADP, SonTek) with the sensor probe facing upward. Currents in the blind spots of the PC-ADP and ADP were measured using Valeport-106 flow sensors (Valeport Ltd, Devon, UK). Water and wave heights were measured using SBE 26 plus SEAGAUGE wave–tide recorders (Sea-Bird Electronics). Surface water was sampled at the Xuliujing (upper estuary) (1998–2001, 2009–2014), Gaoqiao (lower estuary) (2009–2017), and Sheshan (delta front) (2009–2017) stations (Fig. 1B) with 600-mL bottles twice per day (at an interval of 6 h). Water samples were filtered through preweighed 0.45-μm filters, which were rinsed and dried at 45°C for 48 h, and then weighed. SSC was calculated as the ratio of dry suspended sediment weight to filtered water volume. Each annual value of SSC at the three stations was calculated as the yearly average of the SSC values of the 730 or 732 samples. Turbidity profiles were measured at Xuliujing, Gaoqiao, Sheshan, S_1 (marsh), S_2 (mudflat), and S_3 (subaqueous delta) stations during spring, mean, and neap tides (September 2009) using sets of OBS-3A (Campbell Scientific, Logan, UT) and Argus Surface Meter IV (Argus, Germany) sensors. Turbidity signals were then converted into SSC values via calibration with in situ sediment samples. Regression between SSC and turbidity yielded a correlation coefficient greater than 0.99. We established time-averaged SSC profiles at the Xuliujing, Gaoqiao, and Sheshan stations, and calculated the ratios of time-averaged SSC to surface SSC, and then converted the annual values of surface SSC to annual values of depth-averaged SSC using these ratios.

Testing water content and organic matter of sediments

To test the water contents of the sediment samples, we first weighed the wet sediment samples. After the sediment samples were dried at 50°C in an oven for 48 h or more to obtain a stable weight; we reweighed them. We then derived the water content from the ratio of water weight (the difference between wet and dry sediment weights) to dry sediment weights. An oxidation–reduction titration method was used for the determination of organic matter content. This method is suitable for samples with organic carbon contents of less than 15% (Yang 1999).

Calculations of seabed erodibility, sediment transport, and morphological change rate

We calculated the critical shear stress for erosion of sediment (τ_{ce}) using Eq. 1 (Taki 2000):

$$\tau_{ce} = 0.05 + \beta \left\{ \frac{1}{[(\pi/6)(1+sW)]^{1/3} - 1} \right\}^2, \quad (1)$$

where β is an electrochemical anchoring coefficient, s is the specific weight of sediment, and W is the water content of sediment sample. We calculated the combined current–wave bed shear stress (τ_{cw}) using Eq. 2 (Soulsby 1995):

$$\tau_{cw} = \tau_c \left[1 + 1.2 \left(\frac{\tau_w}{\tau_c + \tau_w} \right)^{3.2} \right], \quad (2)$$

where τ_c represents bed shear stress due to currents and τ_w represents bed shear stress due to waves (see Supporting Information Appendix S1 for details).

The rates of sediment erosion and deposition were calculated using Eq. 3 (Mitchener and Torfs 1996; Sanford and Maa 2001; Grabowski et al. 2011) and Eq. 4 (Winterwerp and van Kesteren 2004):

$$R_e = M(\tau_{cw} - \tau_{ce}), \quad \text{for } \tau_{cw} > \tau_{ce}, \quad (3)$$

$$R_d = w_s C, \quad (4)$$

Table 1. Rates of marsh progradation and values of influencing factors in the Yangtze Delta during four periods.

	Influencing factors						Rate of marsh progradation	
	Q_S (Mt yr^{-1})	Q (km^3 yr^{-1})	T_{RS} (m)	L_{SHT} (m)	S_W (m s^{-1})	H_S (m)	$P_{r(a)}$ (ha yr^{-1})	$P_{r(e)}$ (m yr^{-1})
1965–1988 (Stage I)	442	871	3.61	1.88	5.73	0.52	452	162
1988–1995 (Stage II)	362	916	3.63	1.95	5.78	0.52	350	98
1995–2003 (Stage III)	314	974	3.65	2.00	5.84	0.54	250	65
2003–2013 (Stage IV)	140	833	3.66	2.03	5.97	0.55	180	44

Q_S, riverine sediment discharge; Q, riverine water discharge; T_{RS}, spring tidal range; L_{SHT}, level of spring high tide; S_W, wind speed; H_S, significant wave height; $P_{r(a)}$, progradation rate of marsh-area increase; $P_{r(e)}$, progradation rate of marsh-edge advance.

where R_e is the rate of sediment erosion defined as the mass of sediments eroded per unit of time and per unit of bed surface area (kg m^{-2} s^{-1}), M is an erosion constant (kg N^{-1} s^{-1}), R_d is the rate of sediment deposition defined as the mass of sediments that are deposited per unit of time and per unit of bed surface area, w_s is the settling velocity of suspended sediments,

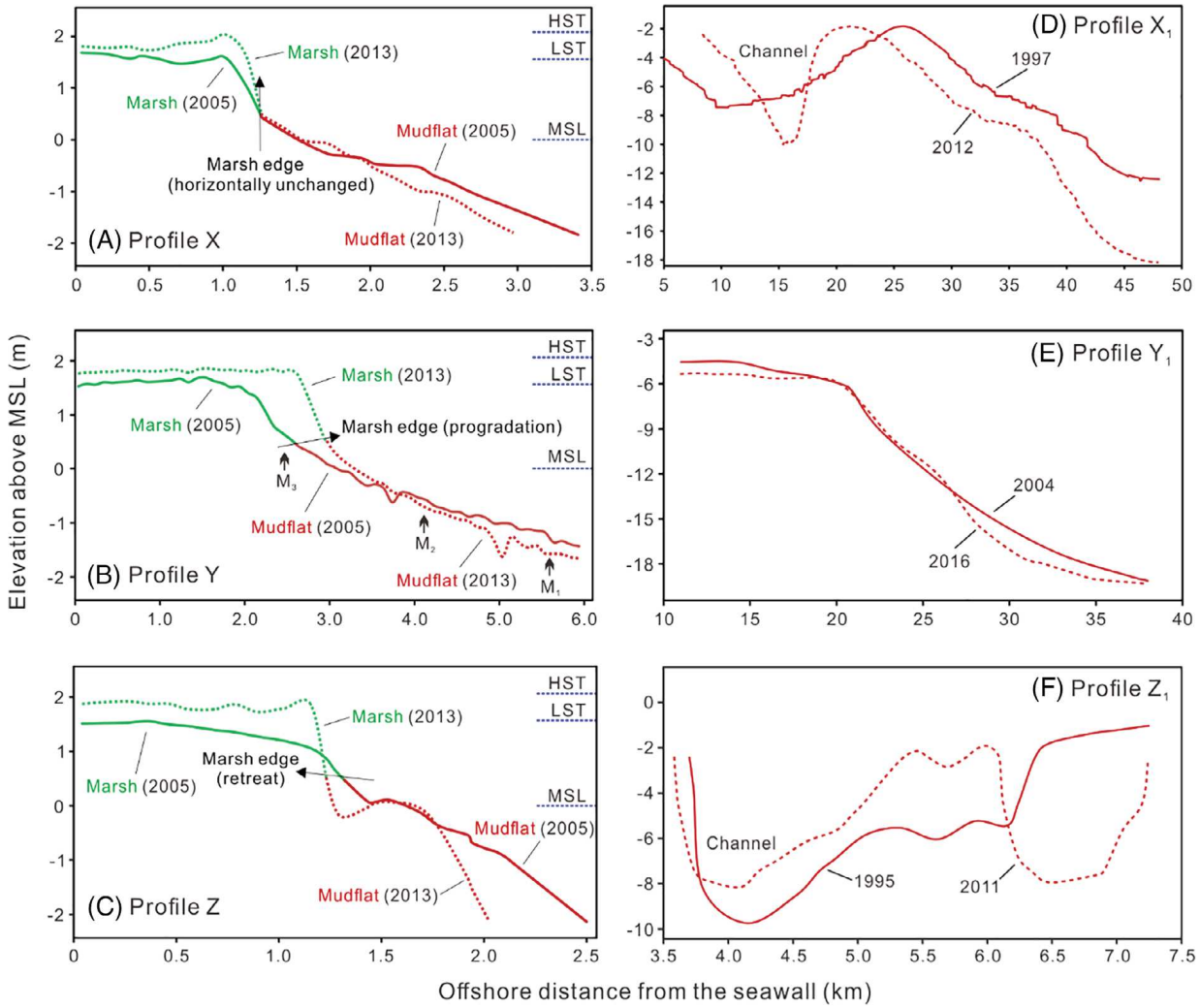

Fig. 3. Decadal changes in cross-shore elevation profiles in the Yangtze Delta. The locations of the transects are shown in Fig. 1B. (**A**–**C**) represent the intertidal wetland profiles (X, Y, and Z), whereas (**D**–**F**) represent the subaqueous delta profiles (X_1, Y_1, and Z_1). Profiles X and X_1 are located on the northeastern coast, Profiles Y and Y_1 are located on the eastern coast, and Profiles Z and Z_1 are located on the southeastern coast. The elevations are expressed relative to the lowest astronomic tide (LAT). HST, high spring tide; LST, low spring tide; MSL, mean sea level. Numbers within the panels represent calendar years. In each panel, the solid line represents the profile surveyed in an early stage, whereas the dotted line represents the profile surveyed in a recent stage. The green lines represent marshes, whereas the red lines represent unvegetated mudflats and subaqueous slopes.

and C represents the SSC (Winterwerp and van Kesteren 2004). The values of M and w_s were calibrated using in situ measurements of bed-level changes in our study area, following the approaches used by Shi et al. (2014).

We calculated the landward and seaward fluxes of sediment transport at the wetland sites by computing the depth-averaged current direction and velocity and SSC, and the landward or seaward component of the product of depth-averaged velocity and SSC, using the vector composition method. Using the ArcGIS 10.5 software package developed by the Environmental Systems Research Institute, we delineated the marsh–mudflat boundaries on the satellite images and the aerial photo photograph, calculated their lengths, and then calculated the area between the marsh–mudflat boundaries in different years, which reflects the net changes during the four periods (1965–1988, 1988–1995, 1995–2003, and 2003–2013). For each period, the areal progradation rate divided by the lengths of the marsh–mudflat boundaries yielded the time-averaged distance progradation rate.

Results

Sea-level rise and fluvial sediment decrease

Between 1965 and 2017, the global mean sea level and the sea level in the Yangtze Delta both showed significant increasing trends, despite interannual fluctuations (Fig. 2A). The results of linear regression are $S_L = 2.398\ Y - 4716$, $R^2 = 0.91$, $p < 0.001$ for the global mean sea level and $S_L = 3.989\ Y - 7845$, $R^2 = 0.88$, $p < 0.001$ for the sea level in the Yangtze Delta, where S_L (in mm) represents the annual mean sea level (relative to the sea level in 1965), Y is the calendar year, R is the correlation coefficient, and p is the significance level. The number preceding Y in the equation reflects the rate of sea-level rise. According to the regression equations, the global mean sea level has risen at a rate of 2.4 mm yr^{-1}, whereas the sea level in the Yangtze Delta has risen at a rate of 4.0 mm yr^{-1}. The rate of sea-level rise in the Yangtze Delta has been greater than the rate of global sea-level rise, because the rate of the warming trend in the Yangtze Delta has been greater than that of the global mean warming trend (SOA 2018). The interannual fluctuations in sea level are attributed to interannual changes in river water discharge, water temperature and atmospheric pressure (SOA 2018). Considering that neotectonic subsidence and sediment compaction in the Yangtze Delta have together resulted in a mean subsidence rate of ~6 mm yr^{-1} (Shi et al. 2009; Wang 2012; Shanghai Municipal Planning and Land Resources Administration 2018), the rate of relative sea-level rise in this delta is ~10 mm yr^{-1}, which falls within the range of the rates of 3–28 mm yr^{-1} reported in previous studies (Syvitski et al. 2009). The discharge of suspended sediment from the Yangtze River into the East China Sea, as measured at the Datong Station (tidal limit), has decreased by more than 70% from > 510 Mt yr^{-1} in the 1960s to < 140 Mt yr^{-1} since the closure of the Three Gorges Dam (TGD), the world's largest dam (Fig. 2B). From 1965–1988 to 2003–2013, the fluvial sediment supply decreased by 68% (within a 95% confidence interval) (Table 1). This magnitude of sediment discharge reduction is larger than reported in earlier studies (e.g., Walling 2006; Dai et al. 2009). Accordingly, the average SSC at Datong declined dramatically from 0.58 kg m^{-3} in the 1960s to only 0.13 kg m^{-3} in the period 2013–2017 (Fig. 2C). More than 90% of the reductions in sediment discharge and SSC are attributable to dam construction, with ca. 20% of the reductions due to the TGD alone (Yang et al. 2018*b*).

Long-term changes in other factors influencing sediment transport and marsh evolution

Over the past five decades, the wind speed, wave height, and tidal range at the Yangtze Delta front (Sheshan Station) have shown gradual increasing trends. The time-averaged wind speed increased from 5.73 m s^{-1} in Stage I (1965–1988) to 5.97 m s^{-1} in Stage IV (2003–2013). The significant wave height increased from 0.52 m in Stage I to 0.55 m in Stage IV. The spring tidal range increased from 3.61 m in Stage I to 3.66 m in Stage IV. As a result of the relative sea-level rise and the increase in tidal range, the high water level of the spring tide increased from 1.88 m in Stage I to 2.03 m in Stage IV. In comparison, the water discharge from the

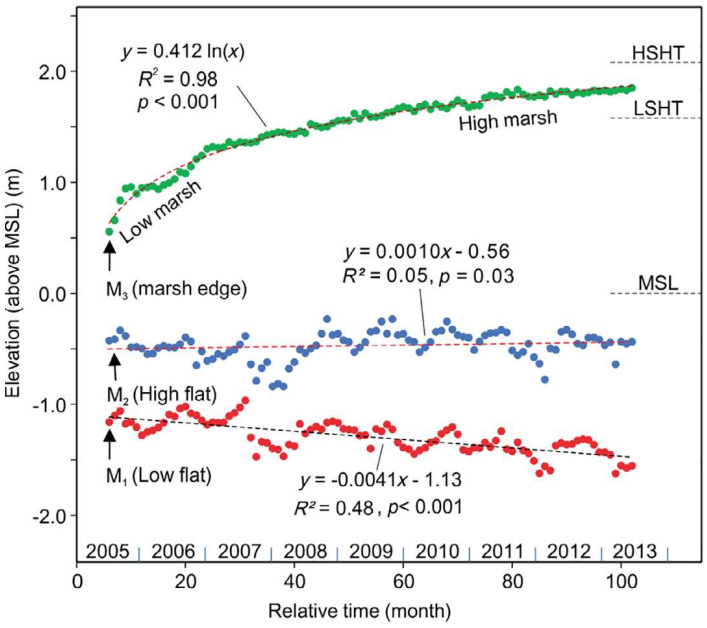

Fig. 4. Monthly changes in elevation at locations on a low marsh edge (M_3), a high flat (M_2), and at a low flat (M_1). Sites M_3, M_2, and M_1 were located 2300, 4100, and 5700 m seaward from the seawall, respectively (see Figs. 1B, 3B for their locations). These elevation changes were based on surveys using the real-time kinematic global positioning system technique. The elevation at M_3 increased from 0.55 m in June 2005 to 1.84 m in June 2013, and the landscape there evolved from a low marsh edge into a high marsh. Sites M_2 and M_1 on the mudflat had original elevations of −0.42 and −1.17 m. Both mudflat sites exhibited seasonal cyclicity of erosion and accretion. The long-term morphological trend at M_2 was slowly accretional, whereas the long-term morphological trend at M_1 was rapidly erosional.

Yangtze River did not show any increasing or decreasing trend. It was 871 $km^3\ yr^{-1}$ in Stage I, 916 $km^3\ yr^{-1}$ in Stage II, 974 $km^3\ yr^{-1}$ in Stage III, and 833 $km^3\ yr^{-1}$ in Stage IV (Table 1). Our long-term measurements of the SSC at the delta front (Sheshan Station) showed a less significant decreasing trend than at upstream locations (Datong, Xuliujing and Gaoqiao Stations) (Fig. 2C).

Marsh vertical accretion and lateral progradation

Between 2005 and 2013, the low marsh edge in the northern cross-shore profile in Eastern Chongming was stable. However, rapid vertical accretion was found within the marsh. The average accretion rate in the marsh profile was 33 mm yr^{-1} (Fig. 3A). Meanwhile, the low marsh edge in the middle cross-shore profile advanced seaward by 370 m (46 m yr^{-1}) due to accretion in the upper mudflat, which led to the expansion of marsh vegetation. The average rate of marsh accretion in the middle profile was 49 mm yr^{-1} (Fig. 3B). In comparison, the low marsh edge in the southern cross-shore profile retreated landward by 90 m (11 m yr^{-1}) due to erosion. The average rate of net marsh accretion in the southern profile was 31 mm yr^{-1} (Fig. 3C). In all the cross-shore profiles, the accretion rates in the low marsh areas were generally higher than the accretion rates in the high marsh areas (Fig. 3A–C). This pattern of decreasing accretion rate with increasing marsh surface elevation was also reflected in the consecutive surveys at a marsh site where the elevation increase decelerated over time (see the elevation sequence at M_3 in Fig. 4). Accretion rates in relatively low-elevation portions of the marsh were five to eight times greater than the local rate of sea-level rise, whereas accretion rates in high-elevation portions of the marsh were similar to the rate of relative sea-level rise ($\sim$13 mm yr^{-1} in Eastern Chongming; Wang 2012). The organic matter contents of core sediments sampled from the marsh deposition layer were less than 2%. Thus, more than 98% of the marsh accretion is attributable to the deposition of mineral particles, and the deposition of organic matter contributes little to the marsh accretion in terms of keeping pace with relative sea-level rise.

The overall rate of lateral marsh progradation (i.e., seaward expansion) has shown a rapid decrease (Fig. 5A). The time-averaged marsh progradation rate decreased by 60% (within a 95% confidence interval) from 452 ha yr^{-1} during 1965–1988 to 180 ha yr^{-1} during 2003–2013 (Table 1). In some places, the seaward marsh progradation has stopped or even reversed, resulting in landward marsh retreat (Figs. 4A,C, 5F). The deceleration of the overall marsh progradation rate correlates closely with the decline in the Yangtze sediment discharge (Fig. 5H). Although this correlation is based on only four data points, the data points represent long-term averages (7–23 years) and the correlation is significant ($p = 0.03$).

Delta-front erosion

Widespread erosion has been observed in the subaqueous delta and the intertidal mudflats on the seaward side of the marshes in Eastern Chongming. Within the last 10–20 years, erosion has occurred in more than 70% of the subaqueous profile extent (within a 95% confidence interval). The total extent of the three subaqueous profiles was 71 km, and the cumulative erosion extent in these profiles was 52 km (Fig. 3D–F). The maximum vertical erosion reaches 5.9 m (0.39 m yr^{-1}) in the northeastern subaqueous profile, 1.6 m (0.13 m yr^{-1}) in the eastern profile, and 6.1 m (0.38 m yr^{-1}) in the southeastern profile (Fig. 3D–F). Between 2005 and 2013, more than 60% of the mudflat profile extent experienced erosion (within a 95% confidence interval). The maximum vertical erosion was ca. 0.5 m (0.063 m yr^{-1}) within the northeastern flat, 0.3 m (0.038 m yr^{-1}) within the eastern flat, and more than 1.1 m (0.18 m yr^{-1}) within the southeastern flat (Fig. 3A–C). The mudflats on the seawards side of the marshes are presently experiencing an average landward retreat of ca. 30 m yr^{-1} (Fig. 3).

Hydrodynamics and sediment transport to the marshes

Contemporary measurements indicate erosion of the seabed in the subaqueous and intertidal mudflat areas at the delta front and transport of the mobilized sediments towards the marshes (Fig. 6). During our observation period, the wind speed was 4.2 ± 1.5 m s^{-1}, which is close to the long-term average wind speed in this delta. The significant wave height at the subaqueous delta observation site was 0.38 ± 0.08 m, and as the water depth was approximately 11 m at this site, the bed shear stress due to waves at this site was low, In contrast, under these conditions, waves in the nearshore portion have the potential to be active and to erode large portions of the shoreline/marsh platform. Consequently, in the shallow water mudflat, the bed shear stress due to waves was high. Thus, the combined current–wave bed shear stress (τ_{cw}) in the subaqueous delta was dominated by tidal currents, whereas τ_{cw} in the intertidal mudflats was determined by both currents and waves (Fig. 6A,B). In the subaqueous delta, the τ_{cw} values during spring tides (with an average tidal range of 3.8 m) exceeded the critical shear stress for erosion of the sediment bed (τ_{ce}) most of the time. In contrast, during neap tides (with an average tidal range of 1.3 m), the τ_{cw} values hardly exceeded the τ_{ce} (Fig. 6A). The SSC during spring tides (0.91 kg m^{-3} on average) was much greater than during neap tides (0.41 kg m^{-3}) (Fig. 6A). The rate of sediment erosion (R_e, occurring only when $\tau_{cw} > \tau_{ce}$) was generally greater than the rate of sediment deposition (R_d) during spring tides, whereas R_e was smaller than R_d during neap tides. The cumulative R_e during spring and neap tides exceeded the cumulative R_d of the same period. The flood currents at the subaqueous delta site were northwesterly toward the coastal wetlands in Eastern Chongming (Fig. 7A).

The salt marshes in Eastern Chongming have formed above the neap high-tide level. Thus, the marshes are submerged only during spring and mean tides. At the mudflat site, τ_{cw} was higher than τ_{ce} for most of the submergence time, and R_e

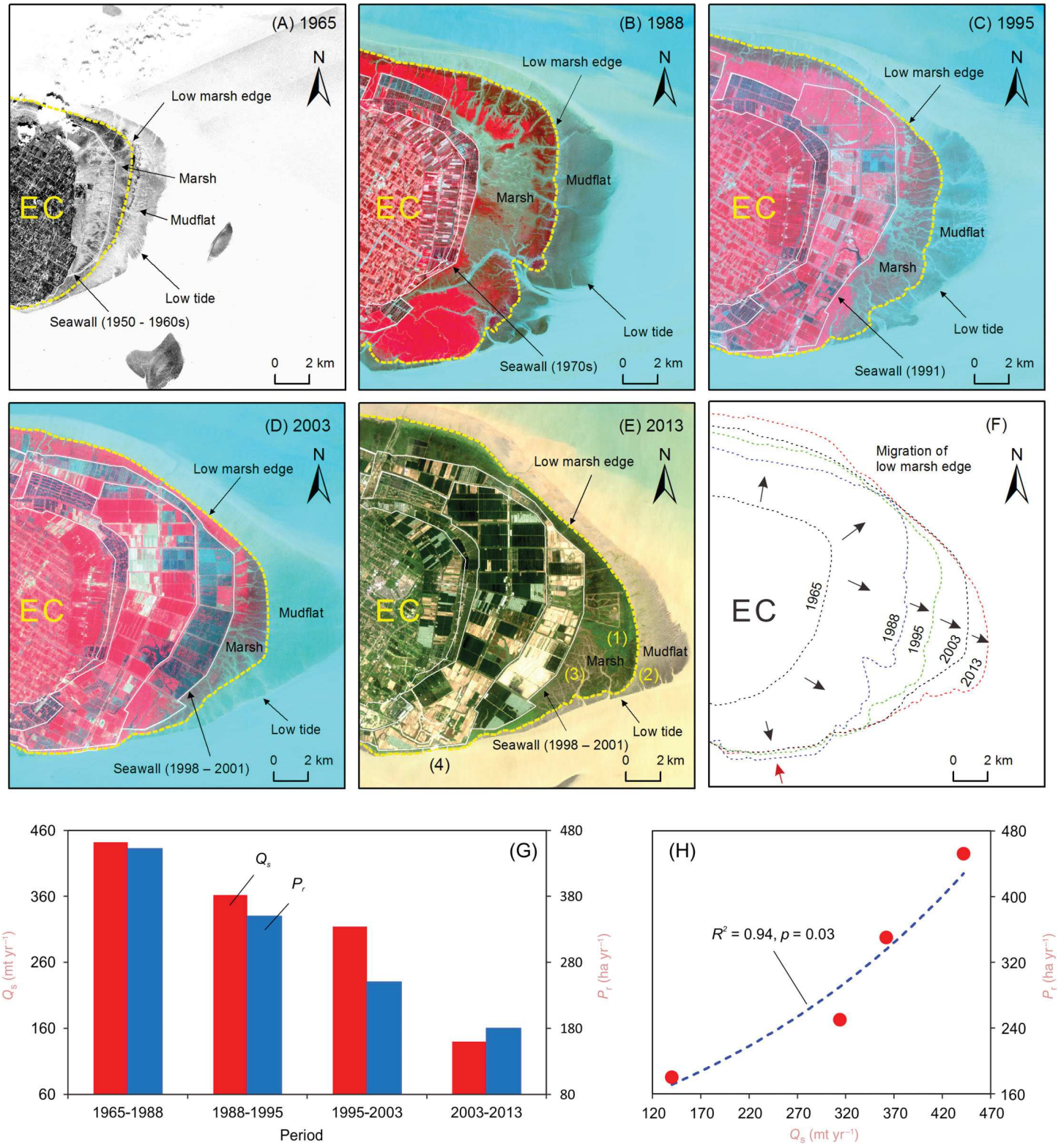

Fig. 5. Reduction in the progradation rate of the marshes in Eastern Chongming (EC) in response to the decline in the sediment discharge of the Yangtze River. (**A**–**F**) Marsh–mudflat boundaries in different years. (**G**) Time-averaged sediment discharge (Q_s) of the Yangtze River and progradation rate (P_r) of salt marshes in Eastern Chongming. (**H**) The correlation between P_r and Q_s in subplot (**G**).

was larger overall than R_d. At the marsh site, however, τ_{cw} was generally lower than τ_{ce}, and R_e was always below R_d. The flood SSC was typically higher than the ebb SSC, and the landward sediment flux into the marsh was greater than the seaward sediment flux out of the marsh, resulting in net marsh deposition (Fig. 6B,C; Table 2).

Sediment budget in the delta

The sediment supply from the Yangtze River during the period 2003–2013 was 140 Mt yr^{-1} (Fig. 2B; Table 1). Meanwhile, the southward longshore currents in the inner continental shelf of the East China Sea transported sediment away from the Yangtze Delta at a rate of ca. 270 Mt yr^{-1}, whereas the sediment transported from the north into the Yangtze Delta by longshore currents was negligible (Deng et al. 2017). There are no accurate estimates of the amount of sediments deposited in the marshes and trapped by coastal engineering projects (i.e., dike structures to promote sediment accretion mainly for subsequent land reclamation) in the Yangtze Delta, but we roughly estimated, based on the sizes and elevation changes of the marshes and engineering areas (Li et al. 2007) and based on a bulk density of 1.3 g cm^{-3}

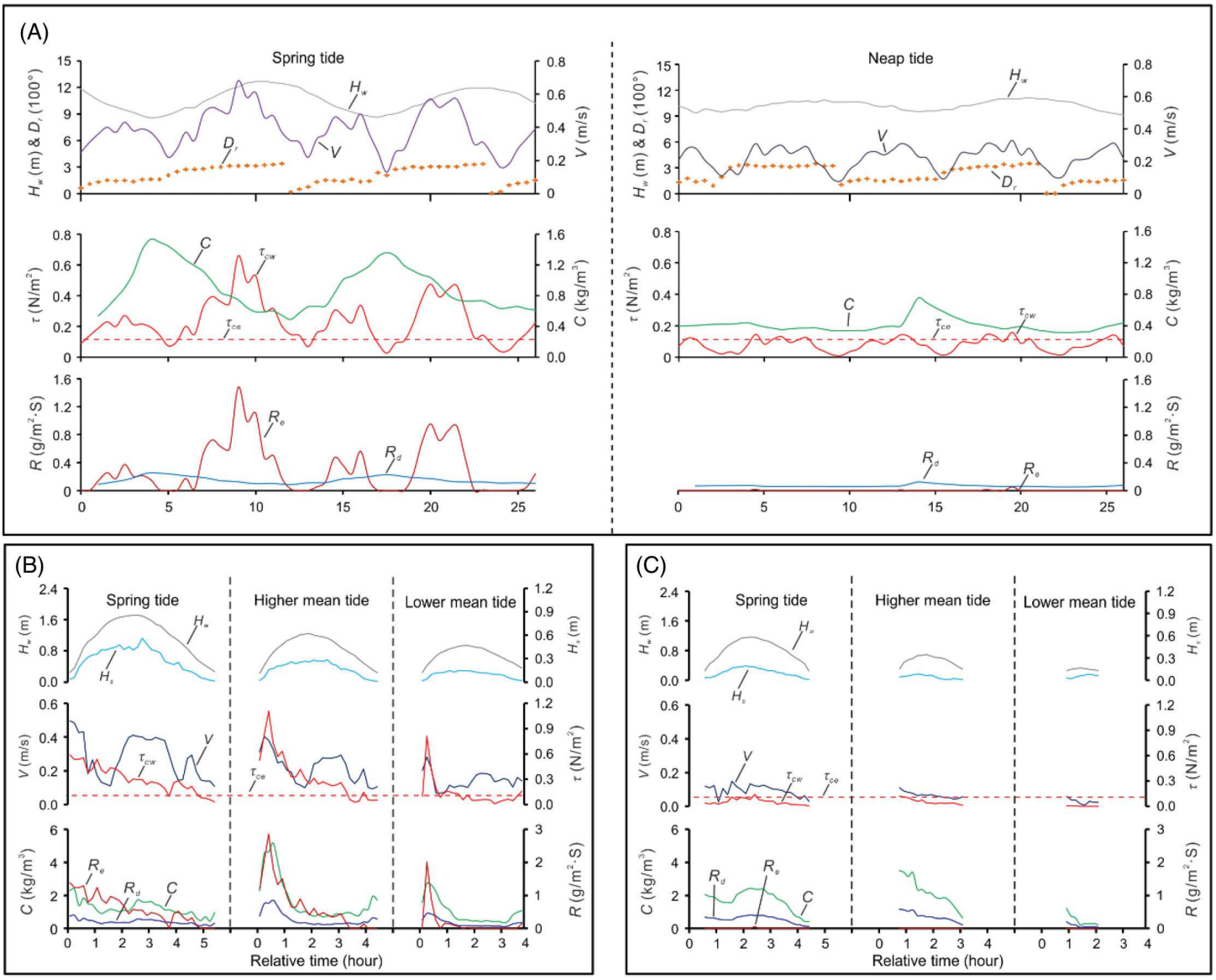

Fig. 6. Time series of water height, flow velocity, bed shear stress, SSC and sediment flux during typical tidal cycles at sites in the subaqueous delta (**A**), mudflat (**B**), and salt marsh (**C**). H_w, water height; H_s, significant wave height; D_r, flow direction; V, near-bed flow velocity; τ_{cw}, combined current–wave bed shear stress; τ_{ce}, critical shear stress for erosion of sediment; C, SSC; R, rate of sediment erosion or sediment deposition. R_e, rate of sediment erosion; R_d, rate of sediment deposition. The wind velocity during the measurement period was 4.2 ± 1.5 m s^{-1} (average ± standard deviation). The tidal ranges during the spring tides, the higher mean tides, the lower mean tides and the neap tides were approximately 3.8, 2.9, 2.6, and 1.3 m, respectively (the measurements were conducted in September 2009).

(Yang et al. 2014), that the total coastal sedimentation reached ca. 100 Mt yr^{-1}. This suggests that approximately 230 Mt yr^{-1} of sediment was provided by delta erosion, which is 1.6 times greater than the fluvial sediment supply (Fig. 7). The sediment transported into the marshes in Eastern Chongming during the flood phase (mainly during spring tides) was derived from the waters on the seaward side (Fig. 6; Table 2). The mean flow velocity in the Yangtze River mouth during spring tides exceeds 1 m s^{-1} (Liu et al. 2014). Thus, the suspended sediments are transported up to 20–30 km during both flood and ebb phases.

Discussion

Mechanisms of salt marsh accretion keeping pace with sea-level rise

Salt marshes develop in the upper portions of the intertidal zone, where sediment deposited on the marsh surface comes principally from mudflats and subtidal areas (Anthony and Dobroniak 2000; Uncles 2002; Mariotti et al. 2010; Ganju et al. 2017). As shown above, the landward sediment flux into the marsh during flood tide tends to be greater than the seaward sediment flux out of the marsh during ebb tide (Table 2). Although bed-level changes reveal seasonal variations in net sediment transport into and out of the mudflats, sediments (partly derived from erosion in the subaqueous delta and the mudflats) are continuously transported into the marshes, resulting in long-term accretion (Fig. 4).

Sedimentation in the intertidal zone can occur through the settling lag/scour lag effects initially identified by Postma (1961) and described in more recent work (e.g., Anthony and Dobroniak 2000; Uncles 2002; van Maren and Winterwerp 2013). The classic theory of Postma (1961) is based on the simplifying assumptions that current velocities at each separate point vary with time as a sinusoidal function and that the current velocities at each stage of the tide decrease from point to point in direct, linear proportion to the distance from the low tide line (Point A). A sediment particle brought into suspension at Point B (on the landward side of A) by the flood current velocity BB′ (representing velocity at B) is carried inland to Point C (on the landward side of B), where the current velocity CC′ (representing velocity at C) equals BB′. Beyond Point C (on the landward side of C) the current velocity drops below the value at which the particle was brought into suspension. The transport of the particle farther inland than Point C can be attributed to two reasons. First, the velocity required to bring a particle in suspension is higher than the velocity necessary to keep the particle in suspension (scour lag). Second, after the current velocity has dropped below the velocity necessary for keeping the particle in suspension, it still takes some time before the particle reaches the bottom (settling lag). As a result, the particle is assumed to reach the bottom at Point D (further landward than Point C). The water mass continues to travel inland to Point E (further landward than Point D) and then returns with the ebb. When it passes Point D again, the water is not able to pick up the particle because the current velocity DD′ (representing velocity at D) is lower than BB′ and CC′. Another water mass, coming from Point F, located further inland than Point E, has exactly the right velocity, as DD″ equals BB′. At the end of the ebb tide this water mass deposits the particle at a Point G between B and C. Hence, over one tidal cycle the particle has been shifted inland over the distance BG. The next tide will cause a further shift inland (fig. 4 in Postma 1961).

The residual landward sediment transport is also associated with tidal asymmetry (van Maren and Winterwerp 2013). In

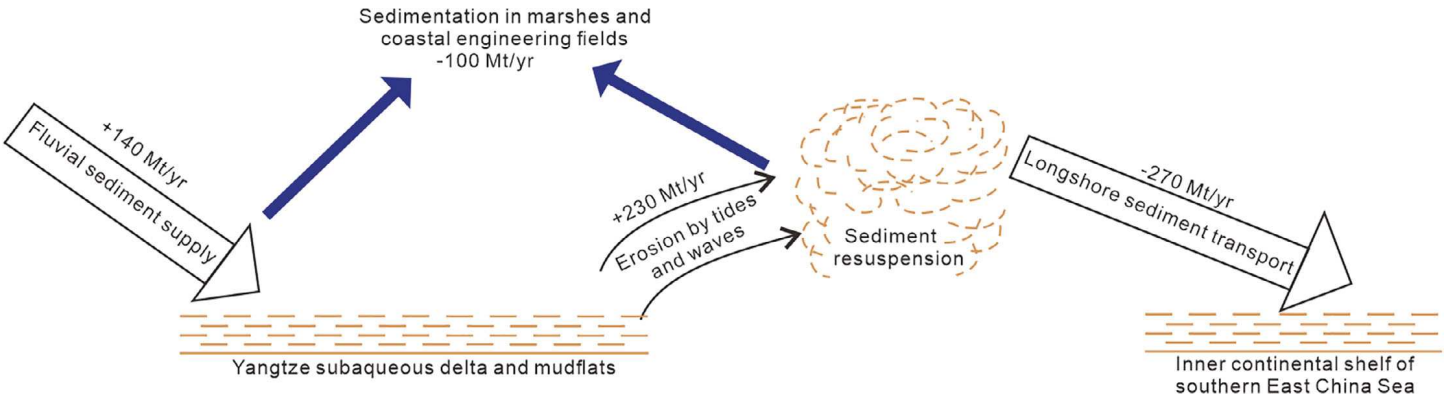

Fig. 7. A schematic diagram showing the sediment budget in the Yangtze Delta under fluvial sediment decline (2003–2013). Positive values indicate sediment inputs into the water body of the delta. Negative values indicate sediment exports from the water body of the delta. Background: The Yangtze sediment discharge has decreased from 5.1 to 1.4 Mt yr^{-1}. The Yangtze Delta is mesomacrotidal and exposed to waves. The combined current–wave bed shear stress tends to exceed the critical shear stress for erosion of the sediment bed. Because of the decline in SSC, the sediment deposition rate tends to be lower than the sediment erosion rate, leading to net erosion in the subaqueous delta and mudflats. A majority of the sediments derived from the river and the seabed erosion are transported away from the delta by the strong southward longshore current, while a minority of the sediments are deposited in salt marshes and coastal engineering fields.

Table 2. Sediment exchange and influencing factors in the tidal wetland in Eastern Chongming during typical tides under normal weather conditions*.

		Mudflat (site S_2)				Marsh (site S_3)			
		Tide 1 (spring tide)	Tide 2 (higher mean tide)	Tide 3 (lower mean tide)	Average	Tide 1 (spring tide)	Tide 2 (higher mean tide)	Tide 3 (lower mean tide)	Average
Water depth at high tide (m)		1.71	1.24	0.94	1.30	1.16	0.69	0.33	0.73
Submergence duration (h)	Flood	2.5	1.92	1.75	2.06	1.83	1.08	0.58	1.22
	Ebb	3.0	2.58	2.08	2.55	2.17	1.42	0.75	1.39
Mean current velocity ($m\ s^{-1}$)	Flood	0.30	0.24	0.13	0.222	0.10	0.081	0.040	0.080
	Ebb	0.27	0.20	0.15	0.208	0.09	0.056	0.020	0.060
Mean significant wave height (m)	Flood	0.34	0.19	0.11	0.21	0.12	0.064	0.03	0.07
	Ebb	0.24	0.16	0.09	0.16	0.09	0.027	0.02	0.05
Mean τ_{cw} ($N\ m^{-1}$)†	Flood	0.43	0.55	0.22	0.40	0.06	0.086	0.004	0.05
	Ebb	0.19	0.16	0.06	0.14	0.05	0.033	0.001	0.03
Mean SSC ($kg\ m^{-1}$‡)	Flood	1.45	2.66	1.46	2.02	1.94	2.96	0.78	1.65
	Ebb	1.15	1.00	0.56	0.90	1.51	1.59	0.27	1.17
Cross-shore sediment exchange ($kg\ m^{-1}$)†	Flood (+)	4700	4640	857	3400	1085	526	19.1	524
	Ebb (–)	3650	1460	471	1860	826	301	4.2	384
	Net exchange	+1050	+3180	+836	+1540	+259	+225	+14.9	+141
Vertical sediment exchange ($kg\ m^{-1}$)†,‡	Deposition (+)	4.20	4.56	2.21	3.66	4.01	3.24	0.39	2.49
	Erosion (–)	11.5	10.9	2.28	8.23	0	0	0	0
	Net exchange	−7.30	−6.34	−0.07	−4.57	+4.01	+3.06	+0.39	2.49

*The wind speed during the observation period was $4.8 \pm 0.99\ m\ s^{-1}$; the tidal ranges of Tide 1, Tide 2, and Tide 3 were 3.5, 2.9, and 2.3 m, respectively.
†The amount of horizontal sediment transport across a meter of shoreline during the tidal cycle.
‡The amount of water-seabed sediment exchange on a square meter during the tidal cycle.

shallow waters, the duration of the flood tide is shorter than that of the ebb tide, and the flow velocity during the flood tide is greater than that during the ebb tide (flood-dominant flow) (Dyer 1997). The ability of the flow to carry sediment is proportional to a second to third power of flow velocity (Parker et al. 1986; Cao et al. 2018). As a result, landward sediment transport during the flood phase tends to be greater than the seaward sediment transport during the ebb phase, unless sediment availability during the flood phase is limited. This theory is supported by our observations in the intertidal wetlands in Eastern Chongming, where the flow velocity, SSC, and sediment transport flux are typically greater during the flood phase than during the ebb phase (Table 2; Fig. 6). Salt marsh deposition is also influenced by vegetation, which attenuates hydrodynamics (Leonard and Luther 1995; Yang et al. 2008; Möller et al. 2014), resulting in $\tau_{cw} < \tau_{ce}$ (Fig. 6C; Table 2), and trapping sediment (Li and Yang 2009).

Of course, the applications of the above theories are subject to some preconditions. One precondition is that the sediment supply from the offshore area is abundant. A second precondition is that the hydrodynamics are determined by the tide. The impact of waves on sediment transport is not considered in these theories. In fact, sediment transport in intertidal wetlands could be more complicated than that considered the above are typically greater. For example, if sediment supply from the offshore area is limited and flood SSC is very low, erosion could occur in the intertidal wetland and the seaward sediment flux in the ebb phase could be greater than the landward sediment flux. This could also occur when wind-driven waves in the ebb phase are larger than those in the flood phase.

The sedimentation rate in a salt marsh is positively related to the flood SSC and the frequency, duration, and depth of tidal inundation (Reed 1995; Kirwan et al. 2010). This theory is supported by our observations that the deposition rate tended to decrease from the low marsh to the high marsh (Figs. 3A–C, 4). When the relative sea-level change is zero, sedimentation progressively increases the elevation of the marsh surface and thereby decreases tidal flooding in the marsh, which in turn reduces sedimentation rate. Ultimately, the marsh is no longer submerged by tides, and no sedimentation occurs in the marsh. Conversely, relative sea-level rise increases tidal flooding and increases the potential for sedimentation, thereby accelerating marsh accretion. Whether

marsh accretion can keep pace with sea-level rise depends on the magnitude of the SSC of the flood water, where the threshold rate of sea-level rise for marsh survival is a positive function of SSC (Kirwan et al. 2010).

Reclamation in estuaries usually increases the tidal range/tidal prism in the adjacent intertidal zones (Anthony and Dobroniak 2000; Pethick and Orford 2013), which would have a similar effect as sea-level rise on sedimentation. Since the 1950s, nearly 10 large-scale reclamation projects have been conducted in Eastern and Northern Chongming Island (Yang et al. 2005; Luo et al. 2017). These activities have likely increased the tidal prism on the marshes in front of the seawalls and increased marsh sedimentation there. The rapid marsh accretion/progradation observed in Eastern Chongming (Figs. 3A–C, 5) could be partly attributed to this mechanism.

Delta-front erosion under fluvial sediment decline provides sediments to prolong marsh survival

Existing knowledge indicates that the fate of a deltaic wetland is largely determined by changes in the sea level and the fluvial sediment supply (Blum and Roberts 2009; Rizzetto and Tosi 2011) and that the future persistence or loss of wetlands can be predicted based on estimates of future rates of sea-level rise and fluvial sediment decrease (Hu et al. 2009; Wang et al. 2014). However, we show that delta erosion on the seaward side of a salt marsh can provide a considerable amount of sediment to sustain the marsh, even under a high rate of relative sea-level rise ($\sim$10 mm yr^{-1}) and a strong reduction in fluvial sediment supply (> 70%).

The huge accretion in the marshes (Fig. 3A–C) was directly attributed to the generally high SSC of the flood water and large net sediment flux into the marsh (Fig. 6; Table 2). Presumably, the sediments deposited in the marshes were partly derived from the delta-front erosion (Fig. 3). This hypothesis is supported by our findings that at the mudflat and subaqueous delta sites, τ_{cw} tended to exceed τ_{ce}, and R_e was generally greater than R_d during spring and mean tides (when the marshes were inundated) under fair weather conditions, suggesting net erosion in the delta front. Previous studies from the Yangtze Delta found that during typhoons coastal waves and τ_{cw} are significantly increased and strong erosion occurs in the mudflats and nearshore zone, resulting in a dramatical increase in flood SSC and rapid deposition in the salt marshes (Yang et al. 2003, 2019). The less significant decreasing trend in SSC at Sheshan Station than at the upstream stations (Fig. 2C) suggests that the delta-front erosion provides sediments to maintain a high level of SSC. Considering that Eastern Chongming is located at the mouth of the Yangtze River (Fig. 1B), the long-term changes in the SSC in Eastern Chongming are presumably intermediate between the dramatic decrease in the SSC at the upstream stations and the lesser decline in the SSC at Sheshan Station.

We infer that the fluvial sediments delivered into the sea during the ebb phase mixed with the sediments derived from seabed erosion, and both were in part transported into the marshes and the engineered sediment-trapping areas and deposited there during the following flood phase. The remaining mixed sediments were transported away from the Yangtze Delta by the residual longshore currents. We argue that the sediments deposited in the marshes and the coastal engineering areas were not derived from the current fluvial sediment source alone, although the coastal deposition was less than the fluvial sediment discharge. Furthermore, we also argue that the sediments transported away from the Yangtze Delta by the longshore currents were not derived from seabed erosion alone. These arguments are based on our understanding of the strong hydrodynamics and sediment mixing at the delta front. The water discharge of the Yangtze River is large (Table 1), and the mesomacrotides lead to high flow velocities (Fig. 7). Furthermore, the waves induced by typhoon and monsoon conditions are usually large (Yang et al. 2019). Therefore, intense widespread water and sediment mixing has been found in the lower Yangtze Estuary and the delta front (Zhang et al. 2007; Liu et al. 2010; Yang et al. 2017). We suppose that the sediments derived from delta-front erosion and the sediments derived directly from the Yangtze River mix with each other and that they together contribute to both the coastal deposition and the longshore sediment transport components. Without erosion in the subaqueous delta front and the mudflats, the deposition in the marshes would have been 60% less than the observed rate. This study supports the previous finding that some parts of a delta can efficiently sequester sediment through the effects of multiple distributary mouths on river-tide-wave interactions, even though other portions of the delta are experiencing erosion (destruction) (Anthony 2015). The Yangtze Estuary is a fine example of multiple distributary mouths (Fig. 1B).

Considering that the temporal changes in water discharge, tidal range, wave height, and sea-level rise rate have been either gradual or fluctuating (Table 1), the rapid decrease in marsh progradation can be mainly attributed to the fluvial sediment decline. However, the decrease in the marsh progradation rate has been slower than the decrease in the fluvial sediment supply (Fig. 5G,H), suggesting that as the fluvial sediment supply decreases to a considerably low level, a new source of sediment has formed to sustain the observed marsh accretion and progradation, and the further the fluvial sediment discharge decreases, the greater the additional sediment supply.

Our findings demonstrating that erosion in certain parts of a delta may contribute to deposition in other parts of the same delta are partly reflected by studies on other deltas. For example, after the loss of the sediment supplied by the Colorado River due to water diversion in the watershed, the eastern portions of its subaqueous delta and the Gulf of California experienced erosion, whereas the western portions experienced deposition (Carriquiry and Sánchez 1999). In response to sediment decline in the Nile, the shoreline retreat of the

promontory was partly counterbalanced by progradation in the adjacent coasts on both sides (Fanos 1995). Similarly, erosion of the Roanoke Delta front and prodelta in the central eastern coast of the United States has acted as a source of sediment to upstream delta plains (Jalowska and Mckee 2017). In the northwestern Gulf of Mexico, the erosion of the Old Brazos Delta became a major source of sediment for the deposition of the adjacent New Brazos Delta (Anderson et al. 2014; Carlin and Dellapenna 2014). In Southeastern Essex, England, sediments eroded from the edge of a marsh were the primary source of sediment for deposition on the marsh surface (Reed 1998). In a Georgia tidal basin, lateral erosion in one part of a salt marsh tends to be counterbalanced by deposition in another part (Frey and Letzsch 1980). However, less is known about the role of nearshore erosion under fluvial sediment decline in delta marsh accretion keeping pace with rapid relative sea-level rise, as observed in the Yangtze Delta. This mechanism is likely of worldwide relevance. Approximately 70% of the world's deltas have experienced a more than 50% reduction in fluvial sediment discharge (Fig. 8; Table S3), and long-term delta-front erosion after a decline in fluvial sediment supply has been widely reported in deltas around the world (Giosan et al. 2014; Anthony et al. 2015; Besset et al. 2017).

Delta erosion may also prolong the persistence of a marsh along the coastline adjacent to the delta, as longshore currents can distribute the eroded sediments away from the delta region. Longshore sediment transport is hardly affected by a declining fluvial sediment supply as long as sediments derived from delta erosion effectively compensate for the decrease in fluvial sediment supply. For example, rapid vertical accretion and lateral progradation are currently observed in the coastal wetlands of Hangzhou Bay, which is located immediately south of the Yangtze Delta (Xie et al. 2017). This mechanism could also be responsible for the formation of large accreting flanking spits due to deposition of sediment eroded from the protruding fronts of several Mediterranean deltas as documented recently by Besset et al. (2017).

Differences in the ability of delta-front erosion to sustain salt marshes among the world's deltas

The ability of delta-front erosion to provide sediment for sustaining marsh accretion under sea-level rise and fluvial sediment decline may be expected to vary largely between deltas for several reasons including differences in hydrodynamic conditions and sediment properties (Bird and Schwartz 1985; Syvitski et al. 2009; Tessler et al. 2015). For example, continued marsh progradation is observed in the Yangtze Delta (Fig. 4), whereas rapid marsh loss is reported in the Mississippi Delta (~7000 km^2, or 25% of the total wetlands, has sunk below sea level over the past few centuries, and an extra 10,000–13,500 km^2 loss is expected by the year 2100) (Blum and Roberts 2009), although the two deltas have experienced similar reductions in fluvial sediment supply and

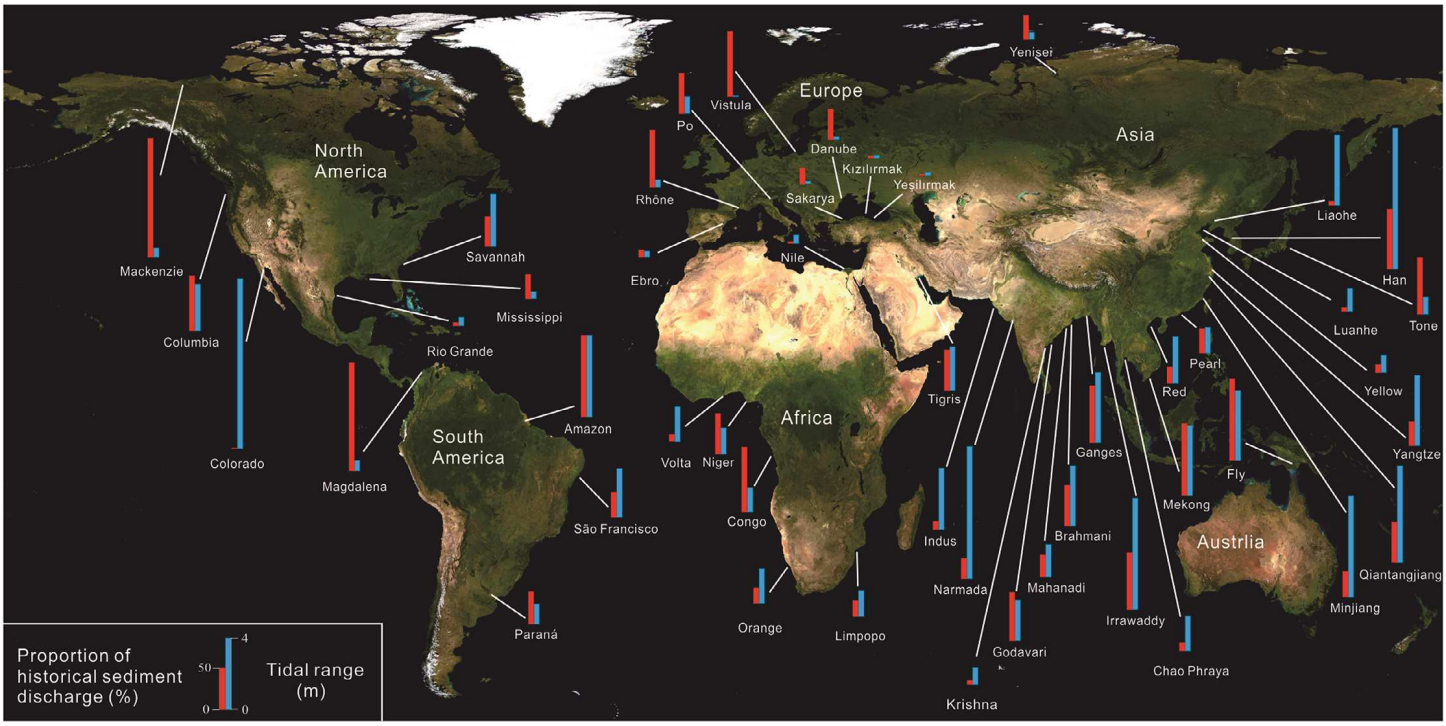

Fig. 8. Present sediment discharges of the world's major rivers expressed relative to the historical values and the spring tidal ranges measured at their deltas. The proportion of historical **s**ediment discharge is given by the percentage of sediment discharge relative to the historical sediment discharge. Larger tidal ranges are associated with a greater ability to resuspend sediment in subaqueous deltas (data and references are presented in Table S3).

rates of relative sea-level rise. The sediment discharges of the Yangtze and the Mississippi rivers both decreased by 70% during the past decades (Table S3). The rates of relative sea-level rise have been 3–28 mm yr^{-1} in the Yangtze Delta and 5–25 mm yr^{-1} in the Mississippi Delta (Syvitski et al. 2009). The tidal range is assumed to be a dominant factor influencing daily sediment resuspension in subaqueous delta areas and tidal advection of this suspended sediment toward deltaic marshes. In the Mississippi Delta, the diurnal tides have a range of ≤ 0.4 m (one order of magnitude lower than in the Yangtze Delta) (Table S3), and wave energy is low most of the time (Wright et al. 1997). The near-bed currents are weak (< 0.1 m s^{-1}), and the τ_{cw} is usually below the τ_{ce} (~0.11 N m^{-2}) (Wright et al. 1997; Xu et al. 2011). Thus, the coastal hydrodynamics in the Mississippi Delta are too weak to resuspend sediments except during storm events (Adams et al. 1987; Xu et al. 2011). As a result, the SSC in the Mississippi Delta is typically low, on the order of 0.01 kg m^{-3} during fair weather conditions and 0.1 kg m^{-3} during storm periods (Wright et al. 1997), which are respectively more than one order of magnitude lower than in the Yangtze Delta (Fig. 6; Liu et al. 2014; Yang et al. 2019). The weak coastal hydrodynamics (mainly because of the microtidal conditions), lower SSC, and shallow submergence (because of the small tidal range) result in marsh deposition that is too slow to keep pace with the rapid relative sea-level rise in most parts of the Mississippi Delta. Extensive marsh loss has been observed in other microtidal systems (Kearney and Turner 2016), most notably the Chesapeake Bay (Stevenson et al. 1985; Schepers et al. 2017; Schieder et al. 2018). As approximately half of the world's deltas have a mesotidal to macrotidal regime similar to that of the Yangtze Delta (Fig. 8; Table S3), we may expect that daily tidal currents can potentially contribute to seabed erosion in the subaqueous delta and mudflat areas and to transport of the eroded sediments toward the salt marshes in these types of delta systems which are threatened by fluvial sediment decline and sea-level rise.

Limits to prolonging marsh survival by delta-front erosion

Salt marshes maintained by sediments derived from delta-front erosion cannot persist forever. It is expected that erosion in subaqueous areas and mudflats results in the steepening of the cross-shore profile of the delta front, as exemplified in the evolution of each topographic profile across the Yangtze Delta (Fig. 3). This process may facilitate the propagation of waves and tidal currents toward the marsh edge and may subsequently hamper the deposition of suspended sediments or even induce erosion of the marsh edge (Reed 1995). Steepening of the cross-shore profile may have contributed to the observed marsh retreat along the southern coast of Eastern Chongming (Figs. 3C, 5F). Vertical accretion rates from the surviving marsh are equal to or greater than the rate of relative sea-level rise (Fig. 3). Therefore, we highlight that delta-front erosion can temporarily provide sediment to maintain marsh accretion, but that lateral erosion is a more prominent threat to marsh persistence. While most previous studies have focused on the vertical balance between accretion and relative sea-level rise (Day et al. 2011; Kirwan et al. 2010), our results contribute to the growing body of evidence from salt marshes that suggests lateral erosion may be a more imminent threat (Mariotti et al. 2010; Kirwan et al. 2016*a*; Ganju et al. 2017), and uniquely suggest that lateral processes are more sensitive than vertical processes to reductions in sediment supply at the scale of one of the world's largest deltas.

The timescales on which delta erosion prolongs marsh persistence may vary among deltas because of differences in coastal processes and in magnitudes of fluvial sediment decline (Fig. 8; Table S3) and relative sea-level rise (Syvitski et al. 2009). In the case of the abandoned Yellow River Delta, the coastal wetlands overall continued prograding between 1855 (since then there has been no sediment supply from the river) and 1900 due to sediment delivered by erosion of the subaqueous delta areas, but the coastal wetlands have receded since 1900. The cumulative net gain of wetland area increased from zero in 1855 to a maximum of 1300 km^2 in 1900 due to coastal progradation, but it decreased back to zero in 1960 due to coastal recession (Zhou et al. 2014). This pattern suggests that delta erosion prolonged coastal wetland persistence by proximately a century in the case of the abandoned Yellow River Delta.

For the Yangtze Delta, we can assume that if the intertidal mudflats and subaqueous delta had not experienced erosion and supplied sediments to the marshes, the marsh progradation in Eastern Chongming would have stopped in 2003 when the TGD began operation. This can be deduced from following estimations. The area of the modern subaqueous Yangtze Delta is ca. 20,000 km^2 (Bird and Schwartz 1985). Annually ca. 0.2 km^3 of deposition is needed to compensate for the 10 mm yr^{-1} relative sea-level rise. Thus, the fluvial sediment discharge needed to sustain accretion at pace with sea-level rise would be ca. 260 Mt yr^{-1}. Considering that the fluvial sediment discharge in 1965–2002 was significantly higher than 260 Mt yr^{-1} and that the fluvial sediment discharge since 2003 has been markedly lower than 260 Mt yr^{-1} (Fig. 2C; Table S2), marsh loss would have been observed since the TGD began operation if no additional sediments had been supplied to the marshes. Because the southward longshore current transports a large amount of sediment away from the Yangtze Delta (Hu et al. 2009; Deng et al. 2017), the beginning of marsh loss is expected to occur earlier than under conditions without the longshore current. We estimate that at the past retreat rate of 30 m yr^{-1} the lateral erosion would reach the low marsh edges in ca. 20 years. Considering the higher sediment compaction in the marshes than in the mudflats and the strengthening of the marsh soil by roots, the lateral erosion in the marshes would presumably be slower than that in the mudflats. Assuming that the marshes would experience an average lateral erosion rate of 15 m yr^{-1}, which is half of the rate in the mudflats, it would take nearly 100 years to erode the marshes that have been formed since the 1990s. Thus, based on this rough assessment, delta-front erosion can probably prolong the marsh persistence in the Yangtze Delta by approximately 150 years.

Implications for other natural systems

Although our research explicitly addresses the evolution of deltas that are vegetated by marshes, we suggest that our findings may also be applicable to other coastal environments, such as mangrove swamps. Like salt marshes, mangrove swamps tend to develop in the upper part of the intertidal zone of deltas, estuaries, coastal lagoons, and bays. Although the vegetation of mangrove swamps (composed of woody plants) is different from salt marshes (composed of grass plants), both systems have similar ecogeomorphic feedbacks, where sediment accretion largely determines their ability to keep up with sea-level rise (e.g., McKee et al. 2007; Krauss et al. 2014; Lovelock et al. 2015). Many deltas with mangroves such as the Indus, Red, Chao Phraya, Irrawaddy, Mekong and Ganges–Brahmaputra deltas are highly impacted by sea-level rise and fluvial sediment decline (Table S3). Differences in above-ground vegetation structure and below-ground root systems of mangroves as compared to salt marshes may lead to quantitatively different behavior (i.e., particular rates of lateral erosion and vertical accretion) under otherwise similar environmental conditions. Nevertheless, it can be generally expected that under favorable conditions, delta-front erosion will also provide sediment to sustain some mangrove swamps.

Conclusions

This study demonstrates that under scenarios of strongly reduced fluvial sediment discharge and rapid relative sea-level rise, the fates of deltaic marshes can be highly variable. We documented a positive interaction on the Yangtze Delta, in which delta-front erosion provides considerable sediment that sustains vertical accretion and lateral progradation (albeit at slower rates than before) in the marsh and temporarily prolongs marsh persistence. However, in locations such as the Mississippi Delta, tides may be too weak to resuspend sediment to maintain marsh accretion at a pace necessary to offset relative sea-level rise. In the long term, continued delta-front erosion and associated steepening of the coastal profile in deltas where tidal action is sufficiently strong to resuspend sediment may facilitate the propagation of waves toward the marsh edge, and therefore reduce marsh progradation and even enhance lateral marsh erosion.

References

Adams, C. E., D. J. P. Swift, and J. M. Coleman. 1987. Bottom currents and fluviomarine sedimentation on the Mississippi prodelta shelf: February-may 1984. J. Geophys. Res. Ocean **92** 14595–609. doi:10.1029/JC092iC13p14595

Anderson, J. B., and others. 2014. Variable response of coastal environments of the northwestern Gulf of Mexico to sea-level rise and climate change: Implications for future change. Mar. Geol. **352** 348–66. doi:10.1016/j.margeo.2013.12.008

Anthony, E. J. 2015. Wave influence in the construction, shaping and destruction of river deltas: A review. Mar. Geol. **361** 53–78. doi:10.1016/j.margeo.2014.12.004

Anthony, E. J., and C. Dobroniak. 2000. Erosion and recycling of estuary-mouth dunes in a rapidly infilling macrotidal estuary, the Authie, Picardy, northern France. Special Publications of the Geological Society of London **175**, 109–121. doi:10.1144/GSL.SP.2000.175.01.10

Anthony, E. J., and others. 2015. Linking rapid erosion of the Mekong River delta to human activities. Sci. Rep. **5** 14745. doi:10.1038/srep14745

Barbier, E. B., and others. 2011. The value of estuarine and coastal ecosystem services. Ecol. Monogr. **81** 169–19. doi:10.1890/10-1510.1

Besset, M., E. J. Anthony, and F. Sabatier. 2017. River delta shoreline reworking and erosion in the Mediterranean and Black Seas: The potential roles of fluvial sediment starvation and other factors. Elementa Sci. Anthrop. **5** 54. doi:10.1525/elementa.139

Besset, M., E. J. Anthony, and F. Bouchette. 2019. Multi-decadal variations in delta shorelines and their relationship to river sediment supply: An assessment and review. Earth Sci. Rev. **193** 199–219. doi:10.1016/j.earscirev.2019.04.018

Bianchi, T. S., and M. A. Allison. 2009. Large-river delta-front estuaries as natural "recorders" of global environmental change. Proc. Natl. Acad. Sci. U.S.A. **106** 8085–92. doi:10.1073/pnas.0812878106

Bird, E. C. F., and M. Schwartz. 1985. The world's coastline. New York: Van Nostrand Reinhold.

Blankespoor, B., S. Dasgupta, and B. Laplante. 2014. Sea-level rise and coastal wetlands. Ambio **43** 996–1005. doi:10.1007/s13280-014-0500-4

Blum, M. D., and H. H. Roberts. 2009. Drowning of the Mississippi Delta due to insufficient sediment supply and global sea-levelrise. Nat. Geosci. **2** 488–91. doi:10.1038/ngeo553

Caldwell, R. L., and D. A. Edmonds. 2014. The effects of sediment properties on deltaic processes and morphologies: A numerical modeling study. Case Rep. Med. **119** 961–82. doi:10.1002/2013JF002965

Cao, H., and others. 2018. A general sediment carrying capacity formula and its analysis. J. Coast. Res. **SI 83** 791–5. doi:10.2112/SI83-129.1

Carlin, J. A., and T. M. Dellapenna. 2014. Event-driven deltaic sedimentation on a low-gradient, low-energy shelf: The Brazos River subaqueous delta, northwestern Gulf of Mexico. Mar. Geol. **353** 21–30. doi:10.1016/j.margeo.2014.03.017

Carriquiry, J. D., and A. Sánchez. 1999. Sedimentation in the Colorado River delta and Upper Gulf of California after nearly a century of discharge loss. Mar. Geol. **158** 125–45. doi:10.1016/S0025-3227(98)00189-3

Church, J. A., and N. J. White. 2011. Sea-level rise from the late 19th to the early 21st century. Surv. Geophys. **32** 585–602. doi:10.1007/s10712-011-9119-1

Costanza, R., and others. 1997. The value of the world's ecosystem services and natural capital 1. World Environ. **25** 3–15. doi:10.1016/S0921-8009(98)00020-2

Dai, S. B., S. L. Yang, and M. Li. 2009. The sharp decrease in suspended sediment supply from China's rivers to the sea: Anthropogenic and natural causes. Int. Assoc. Sci. Hydrol. Bull. **54** 135–46. doi:10.1623/hysj.54.1.135

Day, J., and others. 2011. Sustainability of Mediterranean deltaic and lagoon wetlands with sea-level rise: The importance of river input. Estuar. Coasts **34** 483–93. doi:10.1007/s12237-011-9390-x

Deng, B., H. Wu, S. Yang, and J. Zhang. 2017. Longshore suspended sediment transport and its implications for submarine erosion off the Yangtze River estuary. Estuar. Coast. Shelf Sci. **190** 1–10. doi:10.1016/j.ecss.2017.03.015

Dyer, K. R. 1997. Estuaries: A physical introduction. Chichester: John Wiley & Sons, 195. doi:10.1016/0025-3227(74)90006-1

Fanos, A. M. 1995. The impact of human activities on the erosion and accretion of the Nile Delta coast. J. Coast. Res. **11** 821–33.

French, J. 2006. Tidal marsh sedimentation and resilience to environmental change: Exploratory modelling of tidal, sea-level and sediment supply forcing in predominantly allochthonous systems. Mar. Geol. **235** 119–36. doi:10.1016/j.margeo.2006.10.009

Frey, R. W., and W. S. Letzsch. 1980. Deposition and erosion in a Holocene salt marsh, Sapelo Island. Georgia J. Sediment. Res. **50** 529–42. doi:10.1306/212f7a45-2b24-11d7-8648000102c1865d

Ganju, N. K., and others. 2017. Spatially integrative metrics reveal hidden vulnerability of microtidal salt marshes. Nat. Commun. **8** 14156. doi:10.1038/ncomms14156

Gedan, K. B., B. R. Silliman, and M. D. Bertness. 2009. Centuries of human-driven change in salt marsh ecosystems. Ann. Rev. Mar. Sci. **1** 117–41. doi:10.1146/annurev.marine.010908.163930

Giosan, L., J. Syvitski, S. Constantinescu, and J. Day. 2014. Protect the world's deltas. Nature **516** 31–3.

Grabowski, R. C., I. G. Droppo, and G. Wharton. 2011. Erodibility of cohesive sediment: The importance of sediment properties. Earth Sci. Rev. **105** 101–20. doi:10.1016/j.earscirev.2011.01.008

Guillen, J., and J. A. Jimenez. 1995. Processes behind the longshore variation of the sediment grain size in the Ebro Delta coast. J. Coast. Res. **11** 205–18. doi:10.2307/4298322

Hu, K., P. Ding, Z. Wang, and S. Yang. 2009. A 2D/3D hydrodynamic and sediment transport model for the Yangtze Estuary. China J. Mar. Syst. **77** 114–36. doi:10.1016/j.jmarsys.2008.11.014

IPCC. 2013. Working group I fifth assessment report. Cambridge: Cambridge Univ. Press.

Jalowska, A. M., and B. A. Mckee. 2017. Laceby JP, Rodriguez AB, tracing the sources, fate, and recycling of fine sediments across a river-delta interface. Catena **154** 95–106. doi:10.1016/j.catena.2017.02.016

Jerolmack, D. J. 2009. Conceptual framework for assessing the response of delta channel networks to Holocene sea-level rise. Quat. Sci. Rev. **28** 1786–800. doi:10.1016/j.quascirev.2009.02.015

Kearney, M. S., and R. E. Turner. 2016. Microtidal marshes: Can these widespread and fragile marshes survive increasing climate–sea level variability and human action? J. Coast. Res. **319** 686–99. doi:10.2112/JCOASTRES-D-15-00069.1

Kirwan, M.L., G.R. Guntenspergen, A. D'Alpaos, J.T. Morris, S. M. Mudd, and S. Temmerman. 2010. Limits on the adaptability of coastal marshes to rising sea level. Geophys. Res. Lett. **37**, L23401, doi:10.1029/2010GL045489

Kirwan, M. L., and J. P. Megonigal. 2013. Tidal wetland stability in the face of human impacts and sea-level rise. Nature **504** 53–60. doi:10.1038/nature12856

Kirwan, M. L., S. Temmerman, E. E. Skeehan, G. R. Guntenspergen, and S. Fagherazzi. 2016*a*. Overestimation of marsh vulnerability to sea level rise. Nat. Clim. Chang. **6** 253–60. doi:10.1038/nclimate2909

Kirwan, M. L., D. C. Walters, W. Reay, and J. A. Carr. 2016*b*. Sea level driven marsh expansion in a coupled model of marsh erosion and migration. Geophys. Res. Lett. **43** 4366–73. doi:10.1002/2016GL068507

Krauss, K. W., K. L. McKee, C. E. Lovelock, D. R. Cahoon, N. Saintilan, R. Reef, and L. Chen. 2014. How mangrove forests adjust to rising sea level? New Phytol. **202** 19–34. doi:10.1111/nph.12605

Leonard, L. A., and M. E. Luther. 1995. Flow hydrodynamics in tidal marsh canopies. Limnol. Oceanogr. **40** 1474–84. doi:10.4319/lo.1995.40.8.1474

Li, H., and S. L. Yang. 2009. Trapping effect of tidal marsh vegetation on suspended sediment, Yangtze Delta. J. Coast. Res. **25** 915–30. doi:10.2307/27698386

Li, J. F., and others. 2007. Analysis on the development and evolution of tidal flats and reclamation of land resource along shore of Shanghai city. J. Nat. Resour. **22** 361–71.

Li, Y., Z. Qin, and Y. Duan. 1998. An estimation and assessment of future sea level rise in Shanghai region. Acta Geograph. Sin. **53** 393–403.

Liu, H., Q. He, Z. Wang, G. J. Weltje, and J. Zhang. 2010. Dynamics and spatial variability of near-bottom sediment exchange in the Yangtze Estuary, China. Estuar. Cont. Shelf Res. **86** 322–30. doi:10.1016/j.ecss.2009.04.020

Liu, J., S. L. Yang, Q. Zhu, and J. Zhang. 2014. Controls on suspended sediment concentration profiles in the shallow and turbid Yangtze Estuary. Cont. Shelf Res. **90** 96–108. doi:10.1016/j.csr.2014.01.021

Lovelock, C. E., and others. 2015. The vulnerability of Indo-Pacific mangrove forests to sea-level rise. Nature **526** 559–63.

Luan, H. L., P. X. Ding, Z. B. Wang, and J. Z. Ge. 2017. Process-based morphodynamic modeling of the Yangtze

Estuary at a decadal timescale: Controls on estuarine evolution and future trends. Geomorphology **290** 347–64. doi:10.1016/j.geomorph.2017.04.016

Luo, X. X., S. L. Yang, and J. Zhang. 2012. The impact of the three gorges dam on the downstream distribution and texture of sediments along the middle and lower Yangtze River (Changjiang) and its estuary, and subsequent sediment dispersal in the East China Sea. Geomorphology **179** 126–40. doi:10.1002/eco.1543

Luo, X. X., S. L. Yang, R. S. Wang, C. Y. Zhang, and P. Li. 2017. New evidence of Yangtze delta recession after closing of the Three Gorges Dam. Sci. Rep. **7** 41735. doi:10.1038/srep41735

Ma, Z. J., and others. 2014. Rethinking China's new great wall. Science **346** 912–4. doi:10.1126/science.1257258

Mariotti, G., and others. 2010. Influence of storm surges and sea level on shallow tidal basin erosive processes. J. Geophys. Res. **115** F01004. doi:10.1029/2009JF001326

McKee, K. L., D. R. Cahoon, and I. C. Feller. 2007. Caribbean mangroves adjust to rising sea level through biotic controls on change in soil elevation. Glob. Ecol. Biogeogr. **16** 545–56. doi:10.1111/j.1466-8238.2007.00317.x

Milliman, J. D., and K. L. Farnsworth. 2011. River discharge to the coastal ocean. A global synthesis. Cambridge: Cambridge Univ. Press. doi: 10.1017/CBO9780511781247

Mitchener, H., and H. Torfs. 1996. Erosion of mud/sand mixtures. Coast. Eng. **29** 1–25. doi:10.1016/S0378-3839(96)00002-6

Moeslund, J. E., L. Arge, P. K. Bøcher, B. Nygaard, and J. C. Svenning. 2011. Geographically comprehensive assessment of salt-meadow vegetation-elevation relations using LiDAR. Wetlands **31** 471–82. doi:10.1007/s13157-011-0179-2

Möller, I., and others. 2014. Wave attenuation over coastal salt marshes under storm surge conditions. Nat. Geosci. **7** 727–31. doi:10.1038/ngeo2251

Nardin, W., D. A. Edmonds, and S. Fagherazzi. 2016. Influence of vegetation on spatial patterns of sediment deposition in deltaic islands during flood. Adv. Water Resour. **93** 236–48. doi:10.1016/j.advwatres.2016.01.001

National Oceanic and Atmospheric Administration of USA, 2018. Global mean sea level. Available from https://www.star.nesdis.noaa.gov/sod/lsa/SeaLevelRise/LSA_SLR_timeseries_global.php

Paola, C., and others. 2011. Natural processes in delta restoration: Application to the Mississippi delta. Ann. Rev. Mar. Sci. **3** 67–91. doi:10.1146/annurev-marine-120709-142856

Parker, G., Y. Fukushima, and H. M. Pantin. 1986. Self-accelerating turbidity currents. J. Fluid Mech. **171** 145–81. doi:10.1017/S0022112086001404

Pethick, J., and J. D. Orford. 2013. Rapid rise in effective sea-level in Southwest Bangladesh: Its causes and contemporary rates. Global Planet. Change **111** 237–45. doi:10.1016/j.gloplacha.2013.09.019

Postma, H. 1961. Transport and accumulation of suspended matter in the Dutch Wadden Sea. Neth. J. Sea Res. **1** 148–90. doi:10.1016/0077-7579(61)90004-7

Reed, D. J. 1995. The response of coastal marshes to sea-level rise: Survival or submergence? Earth Surf Process. Landforms **20** 39–48. doi:10.1002/esp.3290200105

Reed, D. J. 1998. Sediment dynamics and deposition in a retreating coastal salt marsh. Estuar. Coast. Shelf Sci. **26** 67–79. doi:10.1016/0272-7714(88)90012-1

Rizzetto, F., and L. Tosi. 2011. Aptitude of modern salt marshes to counteract relative sea-level rise, Venice lagoon (Italy). Geology **39** 755–8. doi:10.1130/g31736.1

Sanford, L. P., and J. P. Y. Maa. 2001. A unified erosion formulation for fine sediments. Mar. Geol. **179** 9–23. doi:10.1016/S0025-3227(01)00201-8

Schepers, L., M. Kirwan, G. Guntenspergen, and S. Temmerman. 2017. Spatio-temporal development of vegetation die-off in a submerging coastal marsh. Limnol. Oceanogr. **62** 137–50. doi:10.1002/lno.10381

Schieder, N. W., D. C. Walters, and M. L. Kirwan. 2018. Massive upland to wetland conversion compensated for historical marsh loss in Chesapeake Bay, USA. Estuar. Coast. **41** 940–51. doi:10.1007/s12237-017-0336-9

Schuerch, M., and others. 2018. Future response of global coastal wetlands to sea-level rise. Nature **561** 231–4. doi:10.1038/s41586-018-0476-5

Shanghai Municipal Planning and Land Resources Administration, 2018. Shanghai geological environmental bulletin. Available from http://www.shgtj.gov.cn/dzkc/dzhjbg/

Shaw, J. B., D. Mohrig, and R. W. Wagner. 2016. Flow patterns and morphology of a prograding river delta. Case Rep. Med. **121** 372–91. doi:10.1002/2015JF003570

Shi, B. W., S. L. Yang, Y. P. Wang, Q. Yu, and M. L. Li. 2014. Intratidal erosion and deposition rates inferred from field observations of hydrodynamic and sedimentary processes: A case study of a mudflat–saltmarsh transition at the Yangtze delta front. Cont. Shelf Res. **90** 109–16. doi:10.1016/j.csr.2014.01.019

Shi, L. G., L. Cai, and L. Y. Shi. 2009. The microscopic characteristics of Shanghai soft clay and its effect on soil body deformation and land subsidence. Environ. Geol. **56** 1051–6. doi:10.1007/s00254-008-1205-4

Soulsby, R. L. 1995. Bed shear–stress due to combined waves and currents. In, M. J. F. Stive, H. J. De Vriend, J. Fredse, L. Hamm, R. L. Soulsby, C. Teisson and J. C. Winterwerp [eds.]Advances in coastal morphodynamics. Delft Hydraulics: Delft, 4–23.

Spencer, T., and others. 2016. Global coastal wetland change under sea-level rise and related stresses: The DIVA wetland change model. Global Planet. Change **139** 15–30. doi:10.1016/j.gloplacha.2015.12.018

State Oceanic Administration (SOA), People's Republic of China, 2018. China sea level bulletin. Available from http://gi.mnr.gov.cn/201905/t20190510_2411195.html

Stevenson, J. C., M. S. Kearney, and E. C. Pendleton. 1985. Sedimentation and erosion in a Chesapeake Bay brackish marsh system. Mar. Geol. **67** 213–35. doi:10.1016/0025-3227(85)90093-3

Syvitski, J. P. M., and others. 2009. Sinking deltas due to human activities. Nat. Geosci. **2** 681–6. doi:10.1038/ngeo629

Syvitski, J. P. M., C. J. Vörösmarty, A. J. Kettner, and G. Pamela. 2005. Impact of humans on the flux of terrestrial sediment to the global coastal ocean. Science **308** 376–80. doi:10.1126/science.1109454

Taki, K. 2000. Critical shear stress for cohesive sediment transport. Proc. Mar. Sci. **3** 53–61. doi:10.1016/S1568-2692(00)80112-6

Temmerman, S., and others. 2013. Ecosystem-based coastal defence in the face of global change. Nature **504** 79–83. doi:10.1038/nature12859

Tessler, Z. D., and others. 2015. Profiling risk and sustainability in coastal deltas of the world. Science **349** 638–43. doi:10.1126/science.aab3574

Törnqvist, T. E., and others. 2008. Mississippi Delta subsidence primarily caused by compaction of Holocene strata. Nat. Geosci. **1** 173–6. doi:10.1038/ngeo129

Uncles, R. J. 2002. Estuarine physical processes research: Some recent studies and progress. Estuar. Coast. Shelf Sci. **55** 829–56. doi:10.1006/ecss.2002.1032

van Maren, D. S. 2005. Barrier formation on an actively prograding delta system: The Red River Delta. Vietnam Mar. Geol. **224** 123–43. doi:10.1016/j.margeo.2005.07.008

van Maren, D. S., and J. C. Winterwerp. 2013. The role of flow asymmetry and mud properties on tidal flat sedimentation. Cont. Shelf Res. **60** S71–84. doi:10.1016/j.csr.2012.07.010

Vörösmarty, C. J., and others. 2003. Anthropogenic sediment retention: Major global impact from registered river impoundments. Global Planet. Change **39** 169–90. doi:10.1016/S0921-8181(03)00023-7

Wagner, W., D. Lague, D. Mohrig, P. Passalacqua, J. Shaw, and K. Moffett. 2017. Elevation change and stability on a prograding delta. Geophys. Res. Lett. **44** 1786–94. doi:10.1002/2016GL072070

Walling, E. D. 2006. Human impact on land: Ocean sediment transfer by the world's rivers. Geomorphology **79** 192–216. doi:10.1016/j.geomorph.2006.06.019

Wang, H., and others. 2011. Recent changes of sediment flux to the western Pacific Ocean from major rivers in East and Southeast Asia. Earth-Sci. Rev. **108** 80–100. doi:10.1016/j.earscirev.2011.06.003

Wang, H., Z. Ge, Y. Lin, and L. Zhang. 2014. Evaluation of the combined threat from sea-level rise and sedimentation reduction to the coastal wetlands in the Yangtze Estuary. China. Ecol. Eng. **71** 346–54. doi:10.1016/j.ecoleng.2014.07.058

Wang, J. 2012. Evaluation of the combined risk of sea level rise, land subsidence, and storm surges on the coastal areas of Shanghai. China. Clim. Change. **115** 537–58. doi:10.1007/s10584-012-0468-7

Wang, Z., and others. 2018. Three-dimensional evolution of the Yangtze River mouth, China during the Holocene: Impacts of sea level, climate and human activity. Earth-Sci. Rev. **185** 938–55. doi:10.1016/j.earscirev.2018.08.012

Weston, N. B. 2014. Declining sediments and rising seas: An unfortunate convergence for tidal wetlands. Estuar. Coast. **37** 1–23. doi:10.1007/s12237-013-9654-8

Winterwerp, J. C., and G. M. W. van Kesteren. 2004. Introduction to the physics of cohesive sediment in the marine environment. Amsterdam: Elsevier.

Wright, L. D., C. R. Sherwood, and R. W. Sternberg. 1997. Field measurements of fairweather bottom boundary layer processes and sediment suspension on the Louisiana inner continental shelf. Mar. Geol. **140** 329–45. doi:10.1016/S0025-3227(97)00032-7

Xie, D., C. Pan, X. Wu, G. Shu, and Z. B. Wang. 2017. Local human activities overwhelm decreased sediment supply from the Changjiang River: Continued rapid accumulation in the Hangzhou Bay-Qiantang Estuary system. Mar. Geol. **392** 66–77.

Xu, K., C. K. Harris, R. D. Hetland, and J. M. Kaihatu. 2011. Dispersal of Mississippi and Atchafalaya sediment on the Texas–Louisiana shelf: Model estimates for the year 1993. Cont. Shelf Res. **31** 1558–75. doi:10.1016/j.csr.2011.05.008

Xu, X., Y. Tan, S. Chen, and G. Yang. 2014. Changing patterns and determinants of natural capital in the Yangtze River Delta of China 2000–2010. Sci. Total Environ. **466–467** 326–37. doi:10.1016/j.scitotenv.2013.07.043

Yang, H. F., S. L. Yang, and K. H. Xu. 2017. River–sea transitions of sediment dynamics: A case study of the tide-impacted Yangtze River estuary. Estuar. Coast. Shelf Sci. **196** 207–16. doi:10.1016/j.ecss.2017.07.005

Yang, H. F., and others. 2018*a*. Recent coarsening of sediments on the southern Yangtze subaqueous delta front: A response to river damming. Cont. Shelf Res. **155** 45–51. doi:10.1016/j.csr.2018.01.012

Yang, H. F., and others. 2018*b*. Human impacts on sediment in the Yangtze River: A review and new perspectives. Global Planet. Change **162** 8–17. doi:10.1016/j.gloplacha.2018.01.001

Yang, S. L. 1999. Sedimentation on a growing Intertidal Island in the Yangtze River Mouth. Estuar. Coast. Shelf Sci. **49** 401–10. doi:10.1006/ecss.1999.0501

Yang, S. L., Q. Y. Zhao, and I. M. Belkin. 2002. Temporal variation in the sediment load of the Yangtze River and the influences of the human activities. J. Hydrol. **263** 56–71. doi:10.1016/S0022-1694(02)00028-8

Yang, S. L., C. T. Friedrichs, P. X. Ding, J. Zhu, and Q. Y. Zhao. 2003. Morphological response of tidal marshes, flats and channels of the outer Yangtze River mouth to a major Storm. Estuaries **26** 1416–25. doi:10.2307/1353417

Yang, S. L., J. Zhang, J. Zhu, J. P. Smith, S. B. Dai, and A. Gao. 2005. Impact of dams on Yangtze River sediment supply to the sea and Delta wetland response. J. Geophy. Res. Earth **110** F03006. doi:10.1029/2004JF000271

Yang, S. L., and others. 2008. Spatial and temporal variations in sediment grain size in tidal wetlands, Yangtze Delta: On the role of physical and biotic controls. Estuar. Coast. Shelf Sci. **77** 657–71. doi:10.1016/j.ecss.2007.10.024

Yang, S. L., J. D. Milliman, P. Li, and K. Xu. 2011. 50,000 Dams later: Erosion of the Yangtze River and its delta. Global Planet. Change **75** 14–20. doi:10.1016/j.gloplacha.2010.09.006

Yang, S. L., and others. 2014. Downstream sedimentary and geomorphic impacts of the three Gorges Dam on the Yangtze River. Earth-Sci. Rev. **138** 469–86. doi:10.1016/j.earscirev.2014.07.006

Yang, S. L., K. H. Xu, J. D. Milliman, H. F. Yang, and C. S. Wu. 2015. Decline of Yangtze River water and sediment discharge: Impact from natural and anthropogenic changes. Sci. Rep. **5** 1258. doi:10.1038/srep12581

Yang, S. L., and others. 2019. Remote impacts of typhoons on the hydrodynamics, sediment transport and bed stability of an intertidal wetland in the Yangtze Delta. J. Hydrol. **575** 755–66. doi:10.1016/j.jhydrol.2019.05.077

Zhang, J., Y. Wua, T. C. Jennerjahn, V. Ittekkot, and Q. Hea. 2007. Distribution of organic matter in the Changjiang (Yangtze River) Estuary and their stable carbon and nitrogen isotopic ratios: Implications for source discrimination and sedimentary dynamics. Mar. Chem. **106** 111–26. doi:10.1016/j.marchem.2007.02.003

Zhou, L., and others. 2014. Coastal erosion as a major sediment supplier to continental shelves: Example from the abandoned Old Huanghe (Yellow River) delta. Cont. Shelf Res. **82** 43–59. doi:10.1016/j.csr.2014.03.015

Acknowledgments

This work was supported by the Ministry of Science and Technology of China (2016YFA0600901, 2016YFE0133700) and the Natural Science Foundation of China (NSFC)—Shandong Joint Fund for Marine Science Research Centers (U1606401). M.L. Kirwan was supported by the National Science Foundation of the United States (award #1654374, 1426981, and 1529245). We thank John D. Milliman for his helpful suggestions. We also thank W.X. Zhang, P. Li, C.S. Wu, J. H. Liu, Y.W. Liu, C.Y. Zhang, H.F. He, H. Wu, and Q. Zhu for the implementation of field measurements.

Conflict of Interest

None declared.

Submitted 22 June 2019
Revised 02 December 2019
Accepted 03 February 2020

Associate editor: Julia Mullarney